RESEARCH INVESTIGATION OF PICOSECOND AND YAG LASER SYSTEMS

REPORT L920479-36
ANNUAL REPORT

PERIOD COVERED: 1 AUG. 1971 TO 31 JULY 1972

PREPARED UNDER CONTACT N00014-66-C0344
SPONSORED BY
ADVANCED RESEARCH PROJECTS AGENCY ARPA ORDER 1806

United Aircraft Research Laboratories

UNITED AIRCRAFT CORPORATION

EAST HARTFORD, CONNECTICUT 06108

RESEARCH INVESTIGATION OF PICOSECOND AND YAG LASER SYSTEMS

REPORT L920479-36
ANNUAL REPORT

PERIOD COVERED: 1 AUG. 1971 TO 31 JULY 1972

PREPARED UNDER CONTACT N00014-66-C0344
SPONSORED BY
ADVANCED RESEARCH PROJECTS AGENCY ARPA ORDER 1806

United Aircraft Research Laboratories

UNITED AIRCRAFT CORPORATION

EAST HARTFORD, CONNECTICUT 06108

Unclassified

1

Security Classification

DOCUMENT CONTROL DATA - R&D

(Security classification of title, body of abstract and indexing annotation must be entered when the overall report is classified)

1 ORIGINATING ACTIVITY (Corporate author) United Aircraft Research Laboratories Silver Lane, East Hartford, Connecticut 06108	2a. REPORT SECURITY CLASSIFICATION Unclassified 2b. GROUP

3. REPORT TITLE

PICOSECOND PULSES AND YAG LASER SYSTEMS

4 DESCRIPTIVE NOTES (Type of report and inclusive dates)

Technical, Annual 1 August 1971 - 31 July 1972

5 AUTHOR(S) (Last name, first name, initial)

Glenn, W. H. and Clobes, A. R.

6. REPORT DATE	7a. TOTAL NO. OF PAGES	7b. NO. OF REFS
	21	87

8a. CONTRACT OR GRANT NO.	9a. ORIGINATOR'S REPORT NUMBER(S)
N00014-66-C-0344 b. PROJECT NO. c. d.	L920479-36 9b. OTHER REPORT NO(S) (Any other numbers that may be assigned this report)

10. AVAILABILITY/LIMITATION NOTICES

11. SUPPLEMENTARY NOTES	12. SPONSORING MILITARY ACTIVITY
	Sponsored by the Advanced Research Projects Agency, and monitored by the Office of Naval Research

13. ABSTRACT

This report discusses the investigation of the frequency stability characteristic of single-frequency Nd:YAG lasers, and of the use of coherent ultrashort pulses for high resolution imaging. Technical Results on the first topic include; ~~(1)~~ The locking of a single-frequency Nd:YAG laser to the bandpass of a high finesse Fabry-Perot interferometer; ~~(2)~~ The utilization of etalon thermal tuning of the laser for course frequency control; ~~(3)~~ The construction of a second single-frequency laser; and (4) The heterodyning of the two single-frequency YAG lasers at a variable frequency offset.

In the area of high resolution imaging, a discussion of the application of microwave synthetic aperture techniques to optical radar is presented as are initial results of an experiment to obtain high optical resolution by doppler processing.

DD FORM 1 JAN 64 1473

Unclassified

14. KEY WORDS	LINK A		LINK B		LINK C	
	ROLE	WT	ROLE	WT	ROLE	WT
Single-Frequency YAG Lasers						
Frequency Stabilization of YAG Lasers						
Optical Heterodyning						
Coherent Imaging						
Synthetic Aperture						
Picosecond Pulses						

INSTRUCTIONS

1. ORIGINATING ACTIVITY: Enter the name and address of the contractor, subcontractor, grantee, Department of Defense activity or other organization *(corporate author)* issuing the report.

2a. REPORT SECURITY CLASSIFICATION: Enter the overall security classification of the report. Indicate whether "Restricted Data" is included. Marking is to be in accordance with appropriate security regulations.

2b. GROUP: Automatic downgrading is specified in DoD Directive 5200.10 and Armed Forces Industrial Manual. Enter the group number. Also, when applicable, show that optional markings have been used for Group 3 and Group 4 as authorized.

3. REPORT TITLE: Enter the complete report title in all capital letters. Titles in all cases should be unclassified. If a meaningful title cannot be selected without classification, show title classification in all capitals in parenthesis immediately following the title.

4. DESCRIPTIVE NOTES: If appropriate, enter the type of report, e.g., interim, progress, summary, annual, or final. Give the inclusive dates when a specific reporting period is covered.

5. AUTHOR(S): Enter the name(s) of author(s) as shown on or in the report. Enter last name, first name, middle initial. If military, show rank and branch of service. The name of the principal author is an absolute minimum requirement.

6. REPORT DATE: Enter the date of the report as day, month, year; or month, year. If more than one date appears on the report, use date of publication.

7a. TOTAL NUMBER OF PAGES: The total page count should follow normal pagination procedures, i.e., enter the number of pages containing information.

7b. NUMBER OF REFERENCES: Enter the total number of references cited in the report.

8a. CONTRACT OR GRANT NUMBER: If appropriate, enter the applicable number of the contract or grant under which the report was written.

8b, 8c, & 8d. PROJECT NUMBER: Enter the appropriate military department identification, such as project number, subproject number, system numbers, task number, etc.

9a. ORIGINATOR'S REPORT NUMBER(S): Enter the official report number by which the document will be identified and controlled by the originating activity. This number must be unique to this report.

9b. OTHER REPORT NUMBER(S): If the report has been assigned any other report numbers *(either by the originator or by the sponsor)*, also enter this number(s).

10. AVAILABILITY/LIMITATION NOTICES: Enter any limitations on further dissemination of the report, other than those imposed by security classification, using standard statements such as:

(1) "Qualified requesters may obtain copies of this report from DDC."

(2) "Foreign announcement and dissemination of this report by DDC is not authorized."

(3) "U. S. Government agencies may obtain copies of this report directly from DDC. Other qualified DDC users shall request through _____."

(4) "U. S. military agencies may obtain copies of this report directly from DDC. Other qualified users shall request through _____."

(5) "All distribution of this report is controlled. Qualified DDC users shall request through _____."

If the report has been furnished to the Office of Technical Services, Department of Commerce, for sale to the public, indicate this fact and enter the price, if known.

11. SUPPLEMENTARY NOTES: Use for additional explanatory notes.

12. SPONSORING MILITARY ACTIVITY: Enter the name of the departmental project office or laboratory sponsoring *(paying for)* the research and development. Include address.

13. ABSTRACT: Enter an abstract giving a brief and factual summary of the document indicative of the report, even though it may also appear elsewhere in the body of the technical report. If additional space is required, a continuation sheet shall be attached.

It is highly desirable that the abstract of classified reports be unclassified. Each paragraph of the abstract shall end with an indication of the military security classification of the information in the paragraph, represented as *(TS)*, *(S)*, *(C)*, or *(U)*.

There is no limitation on the length of the abstract. However, the suggested length is from 150 to 225 words.

14. KEY WORDS: Key words are technically meaningful terms or short phrases that characterize a report and may be used as index entries for cataloging the report. Key words must be selected so that no security classification is required. Identifiers, such as equipment model designation, trade name, military project code name, geographic location, may be used as key words but will be followed by an indication of technical context. The assignment of links, roles, and weights is optional.

UNITED AIRCRAFT CORPORATION
RESEARCH LABORATORIES

Report Number: L920479-36
Annual Technical Report for
the period 1 August 1971 to 31 July 1972

PICOSECOND PULSES AND YAG LASER SYSTEMS

ARPA Order No.	1806
Program Cost Code:	000001E90K21
Contractor:	United Aircraft Research Laboratories
Effective Date of Contract:	1 August 1966
Contract Expiration Date:	31 July 1972
Amount of Contract:	$447,545.00
Contract Number:	N00014-66-C-0344
Principal Investigator:	Dr. Anthony J. DeMaria (203) 565-3545
Scientific Officer:	Dr. Robert E. Behringer
Short Title:	Picosecond Laser Pulses and YAG Laser Systems
Reported By:	W. H. Glenn and A. R. Clobes

Sponsored By
Advanced Research Projects Agency
ARPA Order No. 1806

L-920479-36

Annual Report Under
Contract N00014-66-C-0344

TABLE OF CONTENTS

		Page
I.	INTRODUCTION AND SUMMARY	I-1
II.	SINGLE-FREQUENCY Nd:YAG LASERS	II-1
	Single-Frequency Nd:YAG	II-1
	Frequency Stabilization of the Nd:YAG Laser	II-6
	Single-Frequency Nd:YAG Laser Heterodyne	II-8
REFERENCES	. . . . .	II-10
FIGURES		
III.	DISCUSSION OF COHERENT IMAGING PROBLEMS	III-1
	Synthetic Aperture Techniques	III-1
	Signal Processing	III-6
	Range and Doppler Spreads	III-8
	Signal Design	III-11
	Receiving Systems	III-13
	Glint Points	III-17
REFERENCES	. . . . .	III-19
FIGURES		
IV.	LABORATORY INVESTIGATION OF COHERENT IMAGING TECHNIQUES . .	IV-1
REFERENCE	. . . . .	IV-6
FIGURES		
APPENDIX I	Single-Frequency, Traveling-Wave Nd:YAG Laser	

SECTION I

INTRODUCTION AND SUMMARY

The effort under this contract has involved investigations of the frequency stability characteristics of single-frequency neodymium:YAG lasers and of the application of picosecond laser pulses to imaging radar problems.

Section II of the report, discusses the results of the work on single-frequency YAG lasers. The YAG lasers employed in this investigation incorporated proprietary techniques to obtain single mode, single-frequency operation. The major technical accomplishments have been: (1) the locking of a single-frequency YAG laser to the bandpass of a high finesse Fabry-Perot interferometer, (2) the use of etalon thermal tuning for coarse frequency control, (3) the construction of a second single-frequency laser and (4) the heterodyning of the two single-frequency YAG lasers at a variable frequency offset.

The technique used to obtain single-frequency operation of the YAG laser was developed under corporate sponsorship prior to the initiation of work on this contract. An article describing this technique has been accepted for publication in Applied Physics Letters. This article entitled, "Single-Frequency Traveling-Wave Nd:YAG Laser," by A. R. Clobes and M. J. Brienza has been included as Appendix I of this report.

Section III of the report, discusses the application of picosecond optical pulses to high resolution optical imaging radar. The particular problem discussed is that of obtaining images of distant objects in situations where the resolution or signal levels are insufficient to allow the use of conventional imaging techniques.

The use of coherent signal processing techniques in the microwave region has led to the development of imaging radar systems whose resolution is much better than that determined by the diffraction limit of the transmitting and receiving apertures. These techniques are applicable to situations in which there is relative motion between the observer and the target to be imaged. This motion leads to a doppler shift of the radar return from a point scatterer. For an extended target there will be differential doppler shift between different parts of the target. Similarly, an extended target will display a distribution in range of the radar return. Coherent processing of the doppler information, in conjunction with range

gating, can be used to provide high resolution imaging of the target. Since the image is obtained by range-doppler processing of the return rather than by conventional geometrical optics, there are situations in which the first technique can provide better resolution than the second. Coherent imaging techniques have been applied very successfully to synthetic aperture side-looking radar for terrain mapping and to mapping of the planetary and especially the lunar surfaces. In the former case, the doppler shift is provided by the motion of the aircraft carrying the radar and in the latter by the rotation of the planetary surface with respect to the observer.

These techniques can be extended to the optical region and should allow extremely high resolution imaging. As in the microwave region, the resolution that can be obtained can be better than that obtainable from conventional imaging.

The resolution capability of a coherent imaging radar in the range direction is determined by the reciprocal of the bandwidth of the transmitted signal. The resolution in the cross range direction depends upon the particular configuration being considered, but can ultimately be close to the wavelength of the transmitted signal. Both of these resolution limits are independent of the target range. In contrast to the linear increase of the resolvable spot size with range in a conventional imaging system.

Continuous trains of pulses having durations of the order of 10^{-10} seconds can presently be obtained from mode-locked Nd:YAG lasers at a wavelength of 1.06 microns. This would imply down and cross range resolutions of the order of 1.5 cm and 10^{-4} cm, respectively. CO_2 lasers offer extremely high powers and high efficiency; there are in addition, other considerations which make the operation of an imaging radar more attractive at 10.6 microns that at 1.06 microns. Present CO_2 laser and suitable modulators, however, lack the bandwidth to allow resolution approaching that obtainable with a neodymium laser.

Section IV of this report, discusses some experimental configurations that can be used for doppler processing of optical radar signals. Experimental data are presented that show two dimensional images of a laboratory target that were obtained by doppler processing in combination with a scanning beam.

The development of stable, single-frequency YAG lasers and the locking of these lasers together constitutes a highly significant technical accomplishment and will be important for many of the applications forecast for Nd:YAG lasers.

The extension of micorwave synthetic aperture radar techniques into the optical region should greatly enhance the capabilities of optical radar systems and will allow images of certain types of targets to be obtained that could not be obtained in any other way.

II. FREQUENCY INSTABILITIES IN THE SINGLE-FREQUENCY Nd:YAG LASER

Single-Frequency Nd:YAG

Frequency variation of the single-frequency Nd:YAG laser output is of two types. The first is a "quantized" frequency change in which the laser output jumps from one cavity mode to the adjacent mode. The particular cavity mode which oscillates is determined by the band pass of an intracavity etalon. As the temperature or angle of the etalon changes, the band pass peak shifts in frequency and it is the cavity mode nearest this peak which oscillates.

The second type of frequency variation arises from changes in the cavity mirror spacing due to thermal effects, and to variation in the optical path length due to changes in index of refraction of cavity material. Such index changes result from variation of either the pump power or of the rod cooling rate or from changes in the ambient air temperature of pressure. Both types of frequency instability will be considered in more detail below.

The "quantized" frequency change in the laser output is shown in Fig. II-1 which is a time exposure of the Fabry-Perot display. The laser oscillates in one cavity mode and then jumps to the adjacent mode which is separated by approximately 500 MHz. The deleterious effect of this change is that during the transition the laser will oscillate in both modes simultaneously and the output is no longer at a single frequency. The particular cavity mode which oscillates is determined by the band pass peak of an intracavity etalon. As the temperature or the angle of the etalon changes, the band pass peak shifts in frequency and it is the cavity mode nearest this peak which oscillates. For now consider only the temperature dependence. The effect can be understood by referri to Fig. II-2 , where the etalon transmission characteristic has been intentionally exaggerated. If the temperature of the etalon changes from T_1 to T_2 , the positio of the transmission peak will shift and the laser will oscillate at a new cavity mode which is displaced in optical frequency from the original frequency. Assume that the cavity mode spacing remains constant with a change in the etalon temperature. The shift in the laser operating frequency due to the etalon effect is quantized in the sense that the transmission peak can take an excursion equal to one-half the cavity mode spacing before a frequency change occurs. Another point to be made is that the band pass peaks of the etalon are separated by $c/2n\ell$ where ℓ is the length of the etalon and n is its index of refraction. The laser will oscillate at the cavity mode which is nearest to the band pass peak of the etalon transmission which, in turn, is nearest to the maximum of the laser gain profile curve.

The transmission peak of the etalon formed by a intracavity flat-ended component is at a frequency given by

$$f = q \frac{c}{2n\ell} \tag{1}$$

where: q = a large integer
n = index of refraction
ℓ = length

We assume that both n and ℓ depend on temperature, and that the dependence of n on f can be neglected.

The laser will oscillate at the cavity mode which is nearest in frequency to the etalon transmission peak. Of interest is the temperature tuning characteristic of the transmission peak which is given by:

$$\frac{df}{dT} = -f \left\{ \frac{1}{n} \frac{dn}{dT} + \frac{1}{\ell} \frac{d\ell}{cT} \right\} \tag{2}$$

The coefficient of linear thermal expansion is given by:

$$\alpha = \frac{1}{\ell} \frac{d\ell}{dT} \tag{3}$$

Thus,

$$\frac{df}{dT} = -f \left\{ \frac{1}{n} \frac{dn}{dT} + \alpha \right\} = -\eta f \tag{4}$$

The optical frequency of the transmission peak depends on two terms, one representing the change in index, the other the change in length of the component and the combined effect is given by η which is a material constant.

The intracavity etalon in the laser is made of fused quartz with $\eta = .5 \times 10^{-5}/^{\circ}C$ and therefore df/dt = 1.4 GHz/°C. If the maximum allowable frequency excursion of the transmission peak is $\pm$ 250 MHz, before the laser begins to oscillate at the adjacent cavity mode, the etalon temperature needs to be held to within $\pm$ .18°C. The required temperature stability is achieved by placing the etalon in a commercially available crystal oven.

It is known that the laser rod can also appear as a mode selecting etalon even though the ends of the rod are anti-reflection coated (<.2 percent reflectance). This is apparent from a Fabry-Perot display of the laser output where the optical modes are found to be near multiples of c/2nL where nL is the optical length of the rod. If the band pass peak of the rod etalon determines the cavity mode which oscillates, and if the maximum frequency excursion of this peak is $\pm$ 250 MHz, then the temperature of the laser rod (η = 1.1 x 10^{-5} /°C) needs to be held within $\pm$ .08°C. Holding the rod temperature within this range is very difficult because of fluctuation in the rod cooling water temperature, varying cooling rates between the rod and the water due to water turbulence, and varying thermal input to the rod because of pump lamp variations. For this reason, it is necessary either completely eliminate the rod etalon or to make it a very low finesse etalon compared to another intracavity etalon which can be carefully controlled in temperature.

A change in the laser operating frequency can also result from an angular change of the intracavity etalon with respect to the beam axis of the laser (Ref. II-1). Consider an etalon of length ℓ, refractive index n and inclined to the incident beam at a small angel θ. The internal angle between the light path and the normal to the etalon surface is $\theta' = \theta/n$. The transmission maximum of the etalon is given by:

$$2n\ell \cos(\theta') = M\lambda \qquad M \text{ is an integer} \qquad (5)$$

For small θ',

$$2n\ell\,(1 - \theta^2/2n^2) = M(\lambda_o - \Delta\lambda) \qquad (6)$$

where λ_o is the resonant wavelength for $\theta = 0$; i.e., $2n\ell = M\lambda_o$, and $\Delta\lambda$ is the shift in the transmission peak due to the tilt. It follows that

$$\Delta\lambda = \frac{-\lambda\theta^2}{2n^2} \qquad (7)$$

or

$$\Delta f = \frac{f\,\theta^2}{2n^2} \qquad (8)$$

The angle tuning curve depends only on the index of refraction and not on its length. The angular tuning curve is also quantized in the sense that the transmission peaks must be shifted by more than one-half the cavity mode spacing

before a frequency change will occur. As an example, suppose that the transmission peak can shift ± 250 MHz before the laser jumps to the adjacent cavity mode. The fused quartz etalon (n=1.5) needs to be held rigidly enough so that its angle with respect to the beam axis does not change by more than ± 2 millirad. In tilting the etalon, the optical path length of the cavity changes slightly and this gives rise to a change in the laser operating frequency which is usually negligible. It should be pointed out that even if the intracavity optical component is held perfectly rigid, it is the relative angle between the laser beam axis and the normal to the etalon surface which is important so that any beam wander in angle caused by index changes in the laser rod, for example, could cause an angular tuning effect.

The role of intracavity etalons in determining the frequency stability of a single-frequency laser has been considered. The main effect of etalons is to cause "quantized" frequency changes in which the laser output jumps from one cavity to the adjacent mode due to a shift in the etalon transmission peak. The importance of holding the etalon temperature and angle within narrow limits is apparent. The other aspect of frequency stability in the Nd:YAG laser is that of changes in the cavity frequency due to variation of the cavity length caused by index of refraction perturbations of the material in the laser cavity or from changes in the cavity mirror spacing due to temperature changes in the support structure. This type of frequency variation is shown in Fig.II-3. A small length change $\Delta\ell$ together with a refractive index change in Δn occuring in a fraction f of the total length of the cavity results in a shift in the oscillation frequency given by:

$$-\frac{\Delta f}{f_2} = \left(\frac{\Delta \ell}{\ell} + f\Delta n\right) \qquad (9)$$

The change in frequency with changes in the cavity length ℓ has been separated into two parts: $\Delta\ell/\ell$ represents the change in length of the cavity due to changes in the physical distance between the cavity mirrors, and a part $f\Delta n$ which represents a change in the optical length of the cavity due to index of refraction changes in the cavity medium. The factors which contribute to the $\Delta\ell/\ell$ term are temperature changes in the cavity produced either by variations in the ambient or by variations in the input power to the laser which changes the thermal load on the surrounding cavity structure. For a change in temperature ΔT, $\Delta\ell/\ell$ is simply αT where α is the coefficient of thermal expansion of the spacer material separating the mirrors which make up the optical cavity. The changes in frequency of oscillation caused by $\Delta\ell/\ell$ are relatively slow due to the thermal mass of the spacer material.

The second term in Eq. (9) is due to changes in the optical path length of the cavity due to variation of the index of refraction in the cavity medium. Changes in ambient temperature, pressure, and humidity change n, and therefore, the optical length of the cavity. Another important index change is due to the Nd:YAG laser material which arise from variations of the input power to the laser rod, or changes in the rate of cooling of the rod. These effects and their magnitude are summarized in Table I.

TABLE I

Source of Frequency Change	$\frac{\Delta f}{f}$	Magnitude of Constant
Thermal Expansion of Cavity	$\alpha \Delta T$	$\alpha = 1 \times 10^{-7}/^{\circ}C$
Atmospheric Temperature	$f_a \beta_T \Delta T$	$\beta_T = 9.3 \times 10^{-7}/^{\circ}C$
Atmsopheric Pressure	$f_a \beta_p \Delta P$	$\beta_p = 3.7 \times 10^{-7}/\text{Torr}$
Laser Rod Index Change	$f \frac{dn}{rdt} \Delta T$	$\frac{dn}{dt} = 7.3 \times 10^{-6}/^{\circ}C$

To put this into better perspective, again consider Eq. (9). Substituting for $\Delta \ell / \ell$ and the terms which contribute to Δn (from Table I).

$$\frac{-\Delta f}{f} = (\alpha + f_a \beta_T) \Delta T_c + f_a \beta_p \Delta P + f_n \frac{dn}{dT} \Delta T_R \qquad (10)$$

where ΔT_c is the change of the cavity structure and ambient air temperature, ΔT_R is the change in the laser rod temperature and ΔP is the change in ambient air pressure. For a cavity structure made from invar ($\alpha = 10^{-7}/^{\circ}C$) and for a laser rod which occupies .1 the total cavity length,

$$\frac{-\Delta f}{f} = (10^{-7} + 8.4 \times 10^{-7}) \Delta T_c + 3.3 \times 10^{-7} \Delta P + 7.3 \times 10^{-7} \Delta T_R \qquad (11)$$

At constant pressure, the resultant cavity frequency shift due to ΔT_c is comparable in magnitude to the shift due to ΔT_R. The relative importance of the terms in Eq. (11) can be put in better perspective by realizing that changes in ΔT_c and ΔP occur relatively slowly over a period of tens of minutes and hours and they result in a long term "drift" of the cavity optical frequency. On the other hand, the temperature of the laser rod is the result of a delicate balance between the incident pump power and the cooling rate and this balance can easily be upset by a flicker in the lamp or bubbles in the cooling water. The laser rod temperature can change in a fraction of a second and it is the resultant cavity frequency changes in this time period which can be termed a frequency instability. Progress has been made toward reducing the temperature fluctuation in the laser rod. A comparison of Krypton arc lamps showed the ILC L661 lamp to have excellent amplitude stability with no tendency for arc wander and this is the lamp being used in the single-frequency laser. Even better lamp stability could be expected using tungsten filament lamps but this would be at the expense of the laser output power. Uneven cooling of the laser rod has been reduced by cladding the rod with a thin walled, transparent, fused quartz sleeve (Ref. II- 2) , which extends the entire length of the rod. The sleeve has a thermal damping effect which integrates out any short term temperature fluctuations in the laser rod.

Frequency Stabilization of the Nd:YAG Laser

In order to relax the minimum temperature variation which can be tolerated on the cavity structure, a feedback loop is incorporated to further frequency stabilize the output of the single-frequency Nd:YAG laser. The requirement on the cavity structure and rod temperature are that they occur relatively slowly so that a feedback loop of a reasonable bandwidth can follow these changes. Feedback stabilized lasers incorporate basically the same elements as are utilized in stabilizing oscillators operating at lower frequencies (Ref.II-3). Common to such systems is a null type frequency discriminator which converts deviation in the oscillator frequency from a reference frequency into a modulated ac error signal. The amplitude and phase of the error signal depend on the magntidue and sign of the frequency deviation from the reference. After phase sensitive detection of the error signal, the resultant dc signal is used to drive the oscillator frequency towards the discriminator null frequency. The short term response of such a system depends on the feedback loop bandwidth and the phase sensitive detector sensitivity. The long term stability of the system is no better than the stability of the reference.

Central to a system of this type is the frequency discriminator and since only relative frequency stabilization is of interest the problem is greatly simplified. Such discriminators have been devised which are based on the interference between two differentially delayed beams in a Michelson interferometer type of arrangement(Ref.II-4). The delay may be introduced by differences in geometrical path length or by differences in refractive index. However, Michelson interferometer discriminators are not very attractive when compared to high Q

resonant cavity discriminators. Frequency stabilizers based on the use of high Q cavities have been used extensively in microwave systems since their development by Pound in 1946 (Ref.II-3). Analogous system have been used at optical frequencies; however, due to difficulties in preserving the relative phase in the bridge arms, proposals for using optical cavities as discriminators have generally been based on their power tranmission or reflection properties rather than on their phase characteristics. (Ref. II-5).

Optical cavities suitable for use in a frequency stabilization loop for the Nd:YAG laser are available commercially as scanning Fabry-Perot interferometers (SFP). These instruments, available from Tropel and Coherent Optics and others, are normally used as optical spectrum analyzers (Ref.II-6) for the analysis of the laser optical modes, and without modifications, they are useful as the discriminator in the closed-loop stabilization scheme. The principle of operation is illustrated in Fig.II-4. The center band-pass frequency of the SFP cavity is modulated at an audio rate, and the effect of this on the transmitted laser power is monitored with a photodetector. When the laser output drifts to one side of the reference cavity response, the output will be amplitude modulated at the cavity modulation frequency. On the other side of the reference cavity resonance, a signal of the opposite phase will result. A phase sensitive detector tuned to this audio frequency may be used to derive from the laser output a dc signal whose amplitude is proportional to the deviation from the center of the deviation. The resultant signal, after amplification, may be used to control the frequency of the laser cavity by a PZT driver mirror so that the output is stabilized on the center of the reference cavity response.

The output of the single-frequency Nd:YAG laser was stabilized using a commerically available (Lansing Model 80.210) feedback loop shown in Fig.II-5. The reference cavity was a Coherent Optics Model 470 Fabry-Perot interferometer of 8 GHz free spectral and a finesse of approximately 125. The resultant half width of the cavity resonance is approximately 65 MHz. The frequency discriminant was obtained by dithering the reference cavity center frequency at a 520 Hz rate. Typically a .05 to .1 volt (RMS) dither voltage resulted insufficient modulation of the optical signal for lock-in. The dither voltage could just as well be applied to the PZT mirror on the laser cavity. The dc bias on the SFP is used to initially center the pass-band at the laser operating frequency. A bias change of 40 volts resulted in a scan of one free spectral range, or 8 GHz. The dc signal output of the phase demodulation was amplified and applied to PZT driven mirror on the single frequency laser. A second SFP of 1.5 GHz free spectral range and a finesse of approximately 150 was used to monitor the laser output as is shown in Fig. II-6.

A comparison of the free running and the stabilized laser output is shown in Fig. II-7. Without stabilization, the laser output frequency ranges over approximately ± 60 MHz in a 10 second time period. This frequency shift is due primarily to small changes in the pump power and in the rod cooling rate and with stabilization, the frequency excursions are reduced to ± 15 MHz. The range of frequency excursion over a number of minutes observation period does not change significantly from these values. The laser has remained stabilized for a period up to ½ hour.

Much better stabilization could be expected by using a faster responding feedback loop. This evidence in Fig. 8 where the envelope of the detected 520 Hz modulation signal is shown for a free running laser. The amplitude of the envelope changes as the unstabilized laser output sweeps through the pass-band of the reference cavity. As can be seen, there are frequency components to 10 Hz and above while the feedback loop response is limited to approximately 1 Hz. Of course, as the loop bandwidth is increased, noise and loop stability becomes a problem. The ultimate limit to the loop response is set by the mechanical resonances of the PZT mirror combination.

Single-Frequency Nd:YAG Laser Heterodyne

Heterodyne of the Nd:YAG laser presents special problems in the sense that the gain profile is very broad, spanning a frequency range of approximately 150 GHz. With no etalon in the cavity the laser will oscillate at the cavity mode nearest to theppeak of the gain profile. In practice, however, there usually are an intracavity etalons and the laser will oscillate at the cavity mode which is nearest to the peak of the etalon transmission curve which, in turn, is nearest to the peak of the gain profile curve. Two Nd:YAG lasers, although identically constructed and using rods made from the same boule of raw material could oscillate a number of GHz apart. The maximum the laser frequency can be shifted by PZT movement of a mirror is the cavity mode spacing which for this laser is 300 MHz. There are situations, such as optical heterodyne of two laser sources or laser oscillator-amplifier configurations where it is necessary to shift the laser frequency by an amount greater than that available from mirror movement alone. The temperature or angle variation of an intracavity etalon as discussed previously, can be used to increase the tuning range of the single-frequency Nd:YAG laser. By placing the etalon in a temperature controlled oven, the maximum tuning range is equal to the $c/2n\ell$ frequency of the etalon. For a 1 cm length of used quartz this frequency range is 10.3 GHz which is covered in a temperature range of 7.4° C. If a 1 cm length of calcite were used instead, the $c/2n\ell$ frequency would be 10.1 GHz which would be covered in a temperature change of 24° C. By using a shorter etalon, i.e., one with a larger free spectral range, correspondingly larger tuning ranges could be achieved. The etalon can be used for course frequency adjustment of the laser to within one cavity mode spacing

of the desired frequency. PZT movement of a cavity mirror can then be used for the fine frequency adjust.

The etalon thermal tuning technique for control of the laser operating frequency to within one cavity mode spacing (approximately 500 MHz) was verified by placing the intracavity etalon in a variable temperature oven. A unifrom increase or decrease of the oven temperature resulted in a monotonic shift of the laser frequency from one cavity mode to the adjacent mode as is shown in Fig. II-9. laser was swept over a 2 GHz frequency range, which is the free spectral range of the etalon, using this technique. The slight nonuniformity in the spacing of the observed modes is due to the shift of the cavity mode frequency due to variation of the cavity length during the 2 minute scan. Fine frequency control within the 500 MHz cavity mode spacing was achieved by PZT movement of a cavity of the tuning range has frequently been observed and the reason for it is not understood. Thus, it was verified that the laser output frequency could be continuously varied over a 2 GHz range. It should be mentioned that electrooptic or piezoelectric methods could also be used to vary the length of the intracavity etalon but temperature tuning is in the most convenient in the present experiments.

With frequency control of the laser output it is now possible to heterodyne two single-frequency Nd:YAG lasers at a variable frequency offset using the experimental configuration shown in Fig.II-11. A second laser, identical to the one already operating, was constructed. Both lasers used 3 x 63 mm rods which were cut from the same boule of raw material and it is expected that the peak of the gain curve for the two lasers should be nearly at the same frequency. A Motorola MRD-500 PIN photodiode with a frequency response to approximately 2 GHz was used as the detector. Also available is a Philco L 4501 diode which has a response to 10 GHz. The photodiode output was displayed on an HP 8551B spectrum analyzer. On heterodyning the output from the two lasers a beat signal at approximately 1.6 GHz was immediately observed. The difference frequency was then varied from approximately 10 MHz (the minimum useful frequency of the spectrum analyzer) to 2 GHz by temperature tuning of one etalon and PZT mirror movement. A typical beat signal is shown in Fig.II-12. The stability of the resultant signal was approximately $\pm$ MHz over a 10 second observation period and this is consistent with the Fabry-Perot display where each oscillator varies over a $\pm$ 60 MHz range during the same observation period. It was verified that the two lasers operate well within the etalon thermal tuning range.

Initial attempts to lock the two lasers together at a zero frequency offset were unsuccessful using a Lansing Model 80.210 lock-in stabilizer. This unit, which had been used to lock the laser output to a stable Fabry-Perot frequency reference, does not have adequate bandwidth. In the next attempt, one laser will be stabilized by locking it to the Fabry-Perot reference cavity and the second laser will then be locked to this stabilized laser.

REFERENCES

II- 1. Hercher, M: Appl. Optics, 8, 1163 (1969).

II- 2. Chester, R.: Applied Optics, 9, 2190 (1970).

II- 3. Pound, R.: Rev. Sci. Inst., 17, 490 (1946).

II- 4. Ballik, E.: Phys. Letters, 4, 173 (1963).

II- 5. White, A.: Rev. Sci. Instis., 38, 1079 (1967).

II- 6. Hercher, M.: Appl. Optics, 7, 951 (1968).

INTRAMODE FREQUENCY INSTABILITY

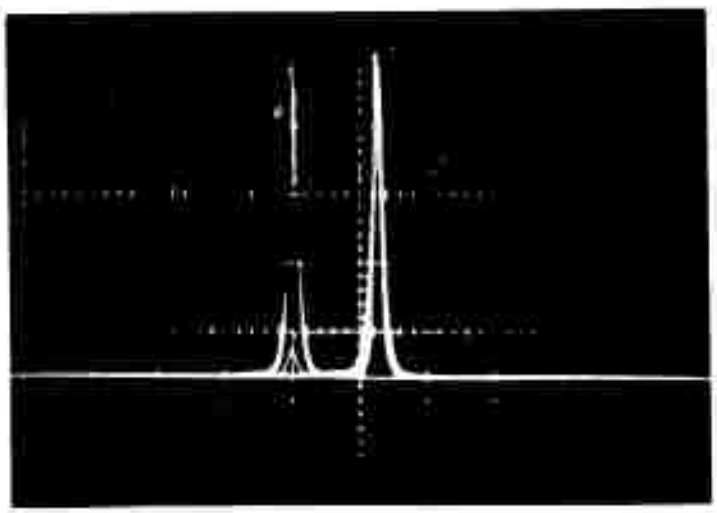

390 MHz /div

FIG. II-2

ETALON THERMAL TUNING CHARACTERISTIC

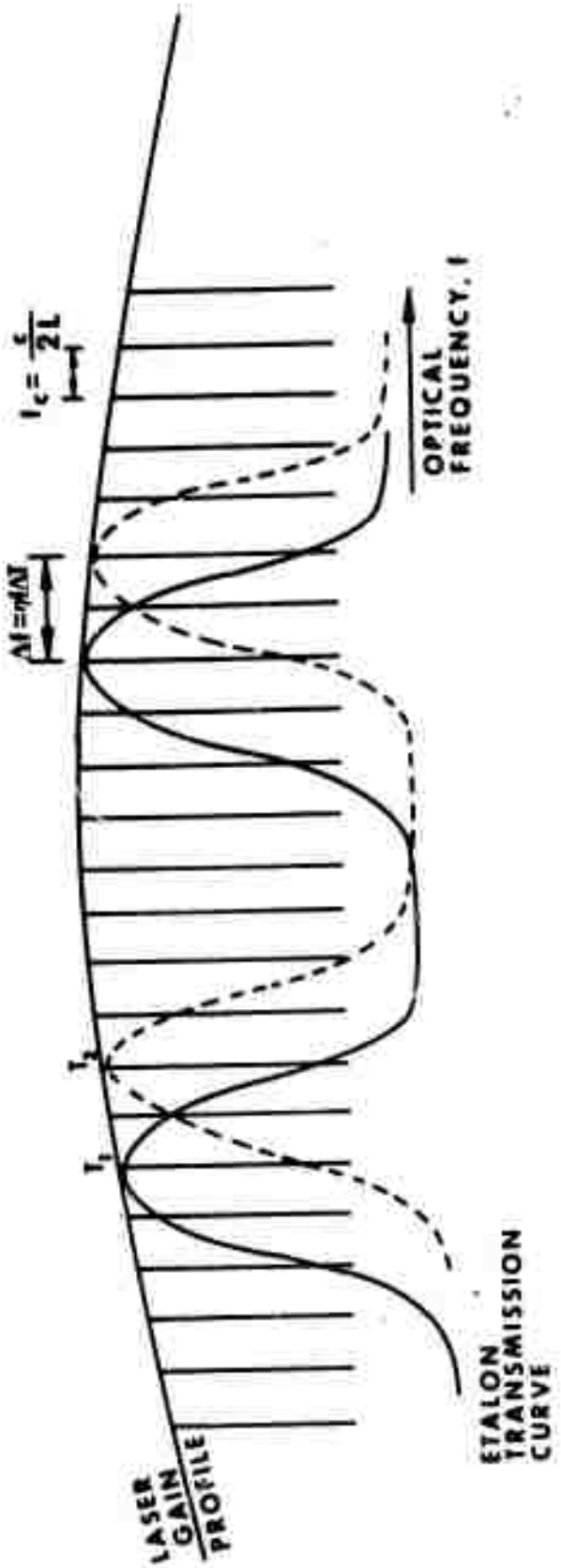

INTERMODE FREQUENCY INSTABILITY

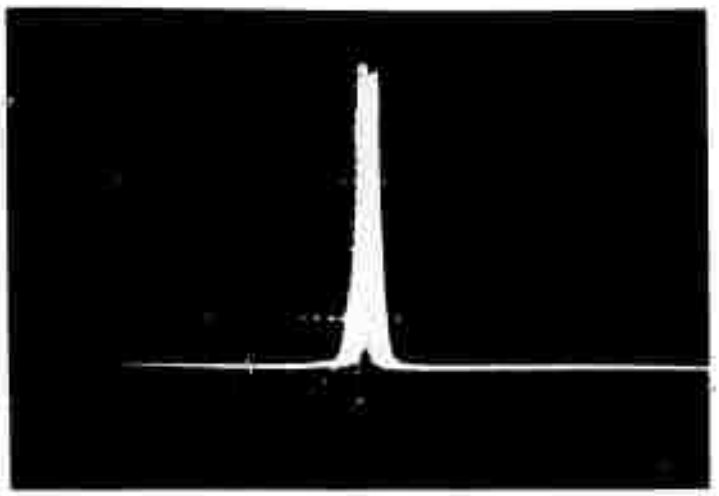

390 MHz /div

FIG. II-4

REFERENCE CAVITY RESPONSE

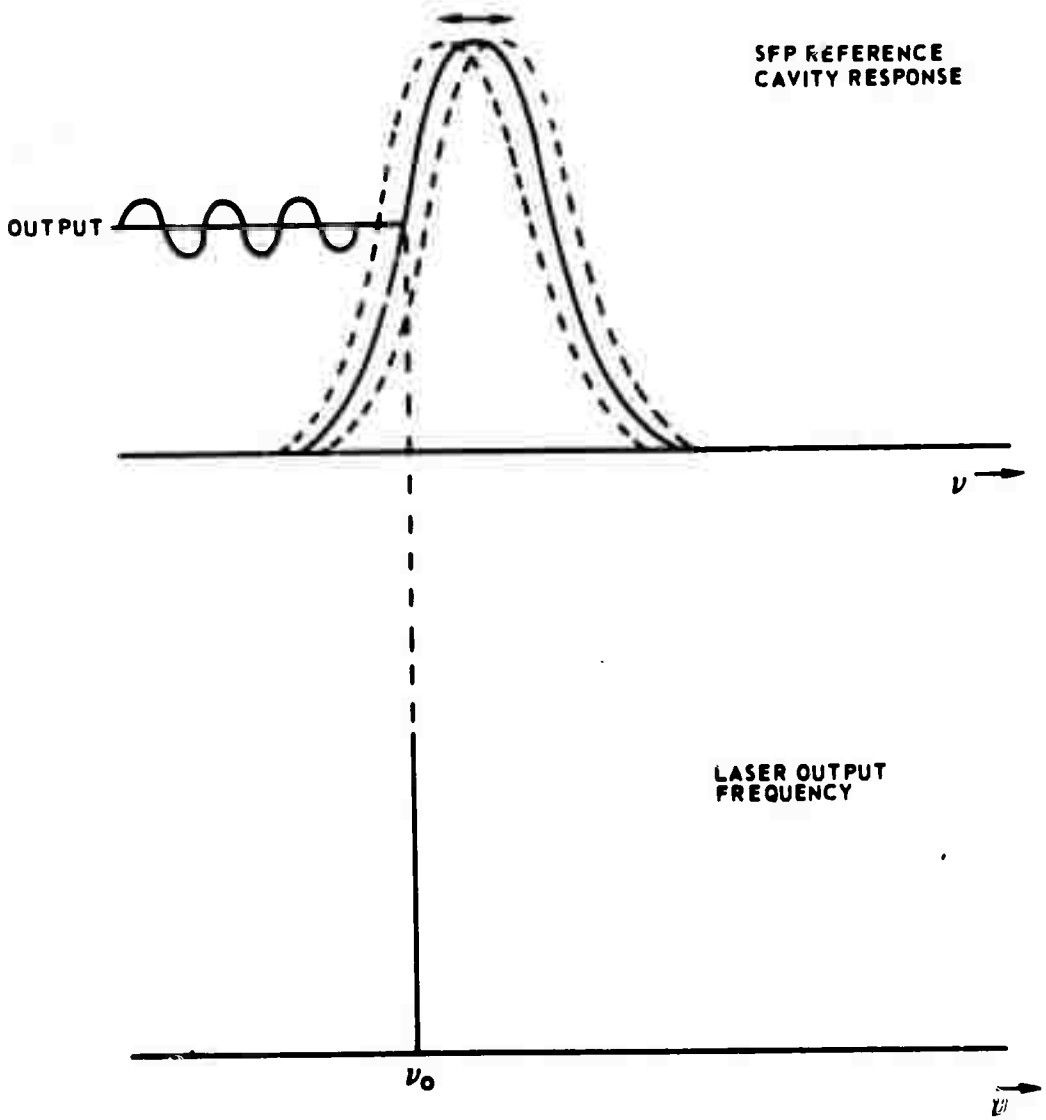

L920479-36

FIG. II-5

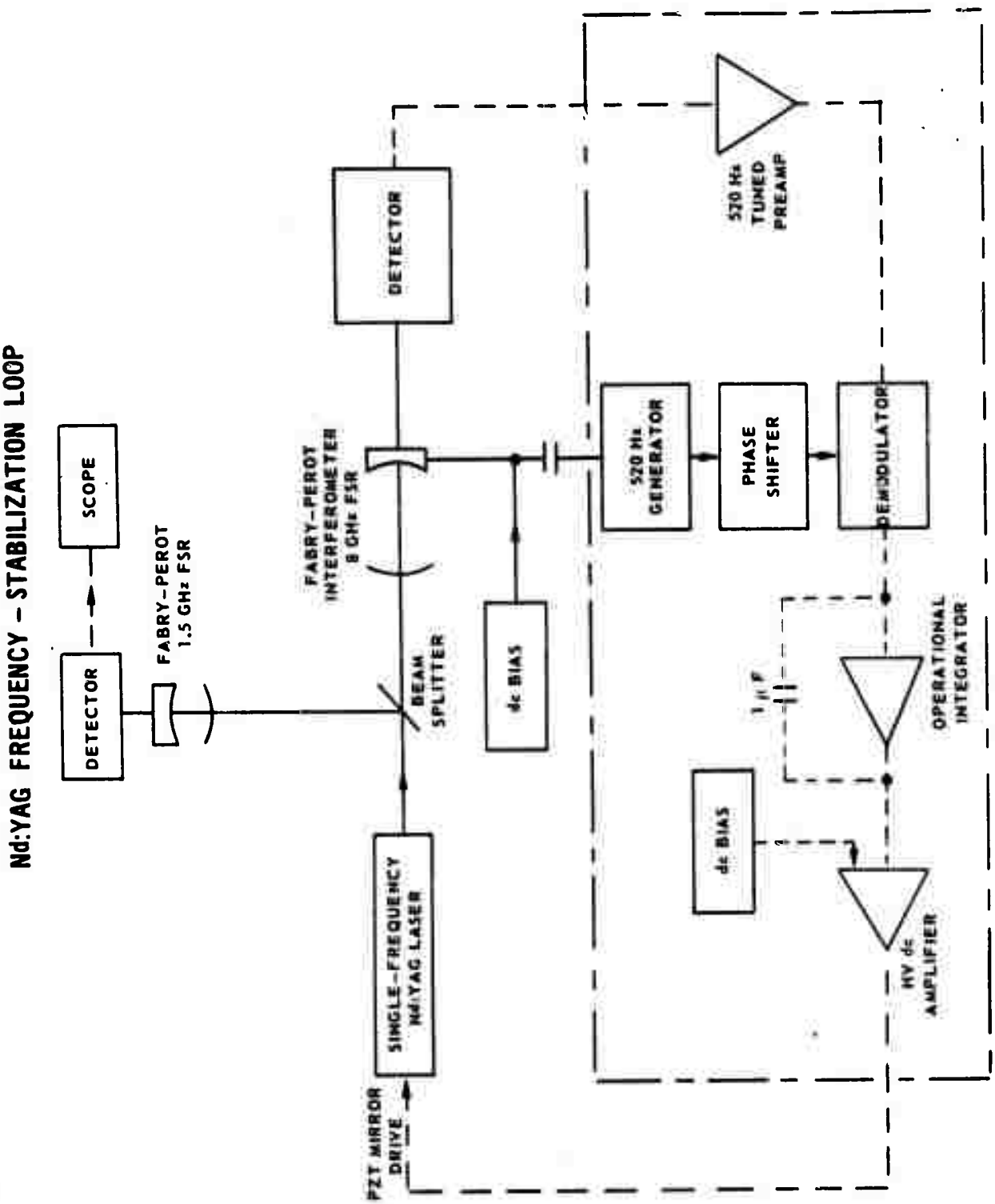

SINGLE-FREQUENCY OUTPUT

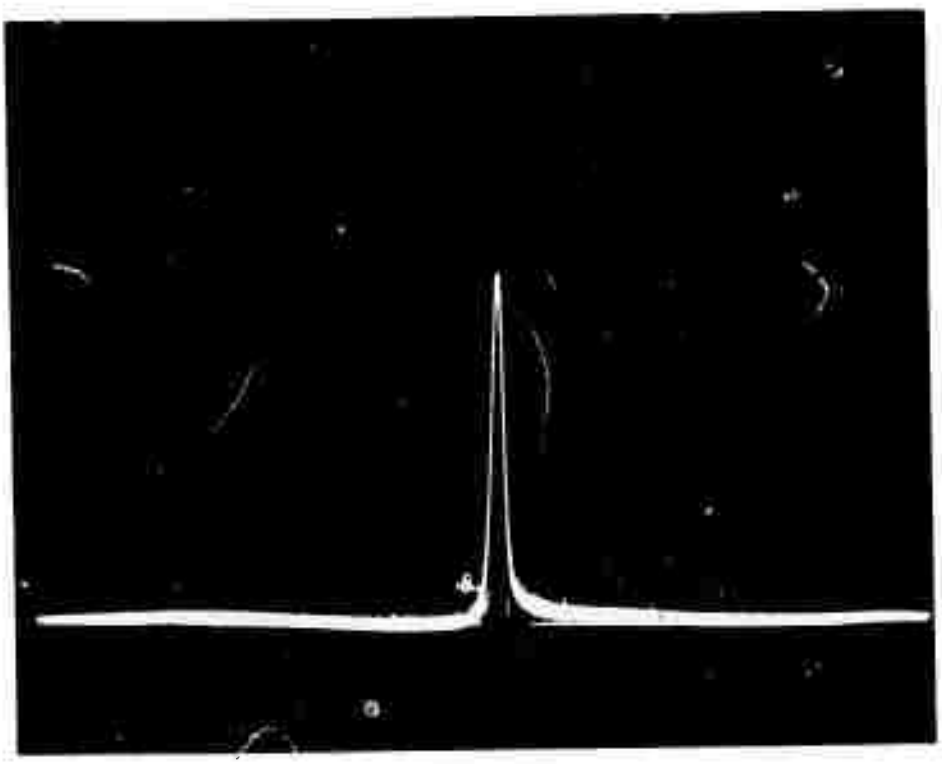

57 MHz/div

STABILIZED SINGLE-FREQUENCY Nd: YAG LASER

10 sec EXPOSURE

57 MHz/div

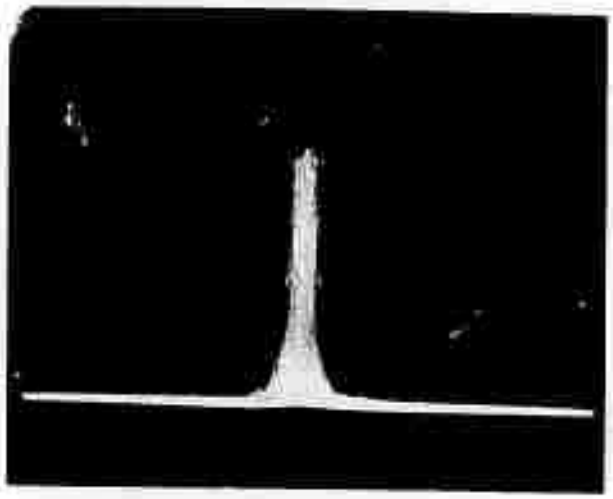

a) LASER STABILIZED

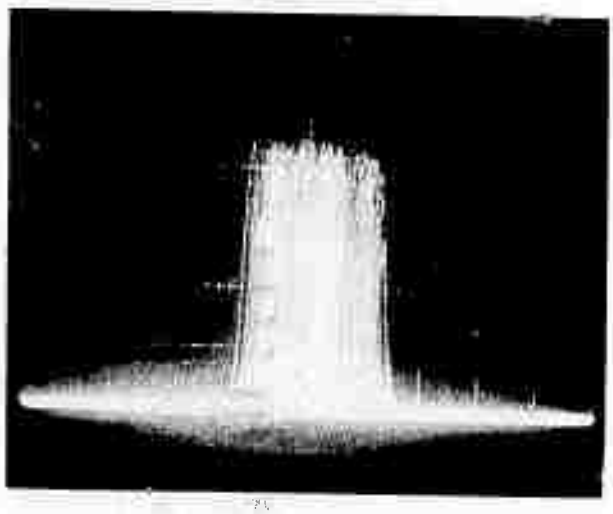

b) LASER FREE-RUNNING

520 Hz AMPLIFIER OUTPUT

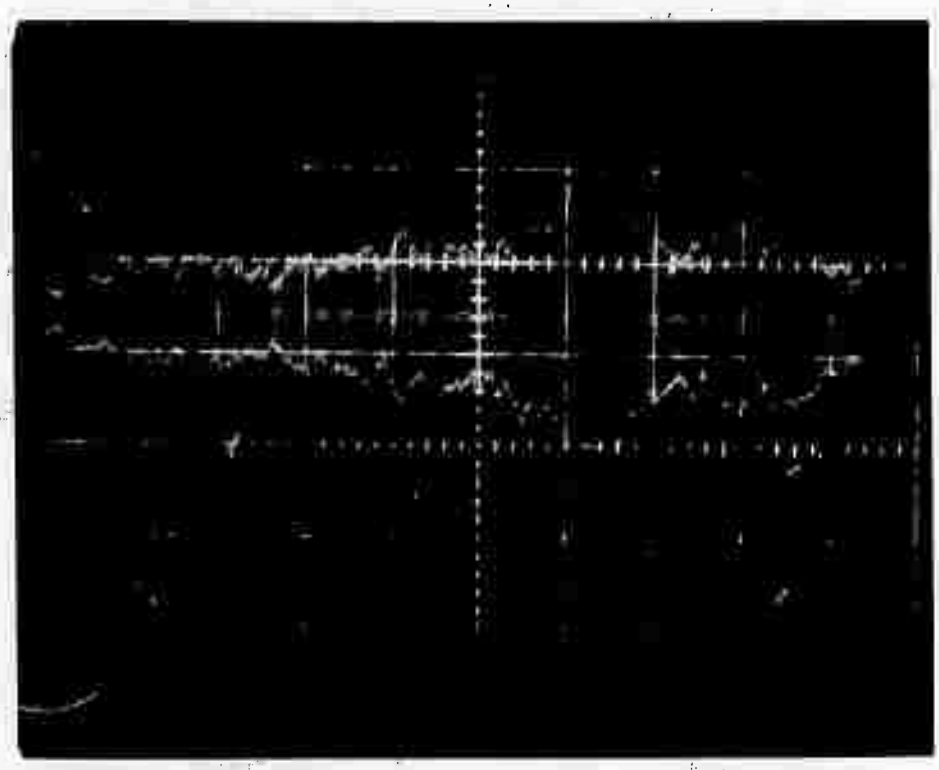

LINEAR SCALE

0.2 sec/div

TEMPERATURE TUNING OF Nd:YAG LASER

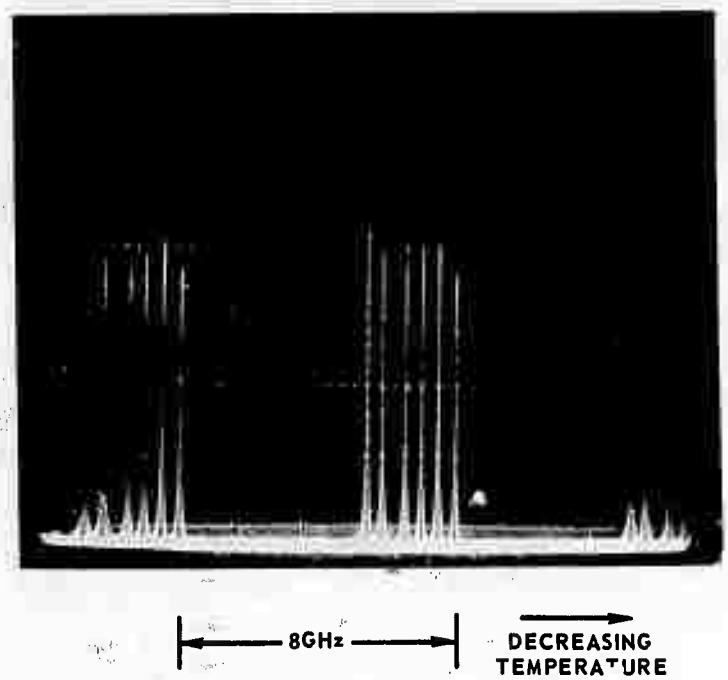

PZT MIRROR-TUNING OF Nd:YAG LASER

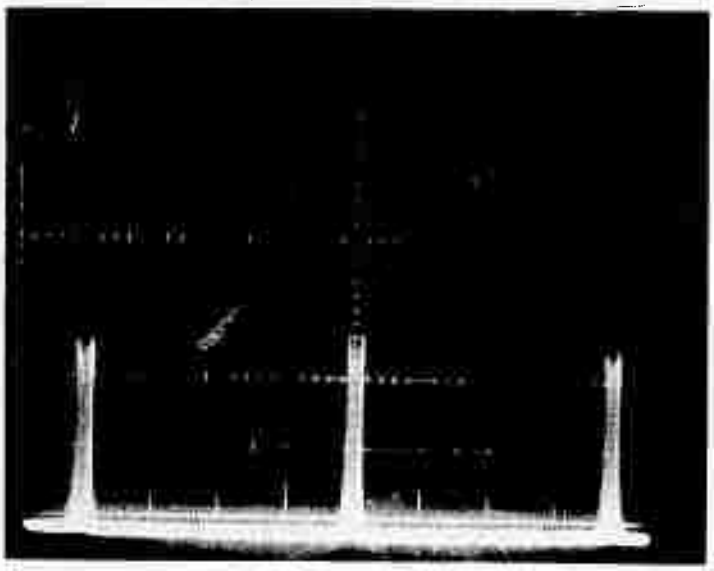

8 GHz

FIG. II-11

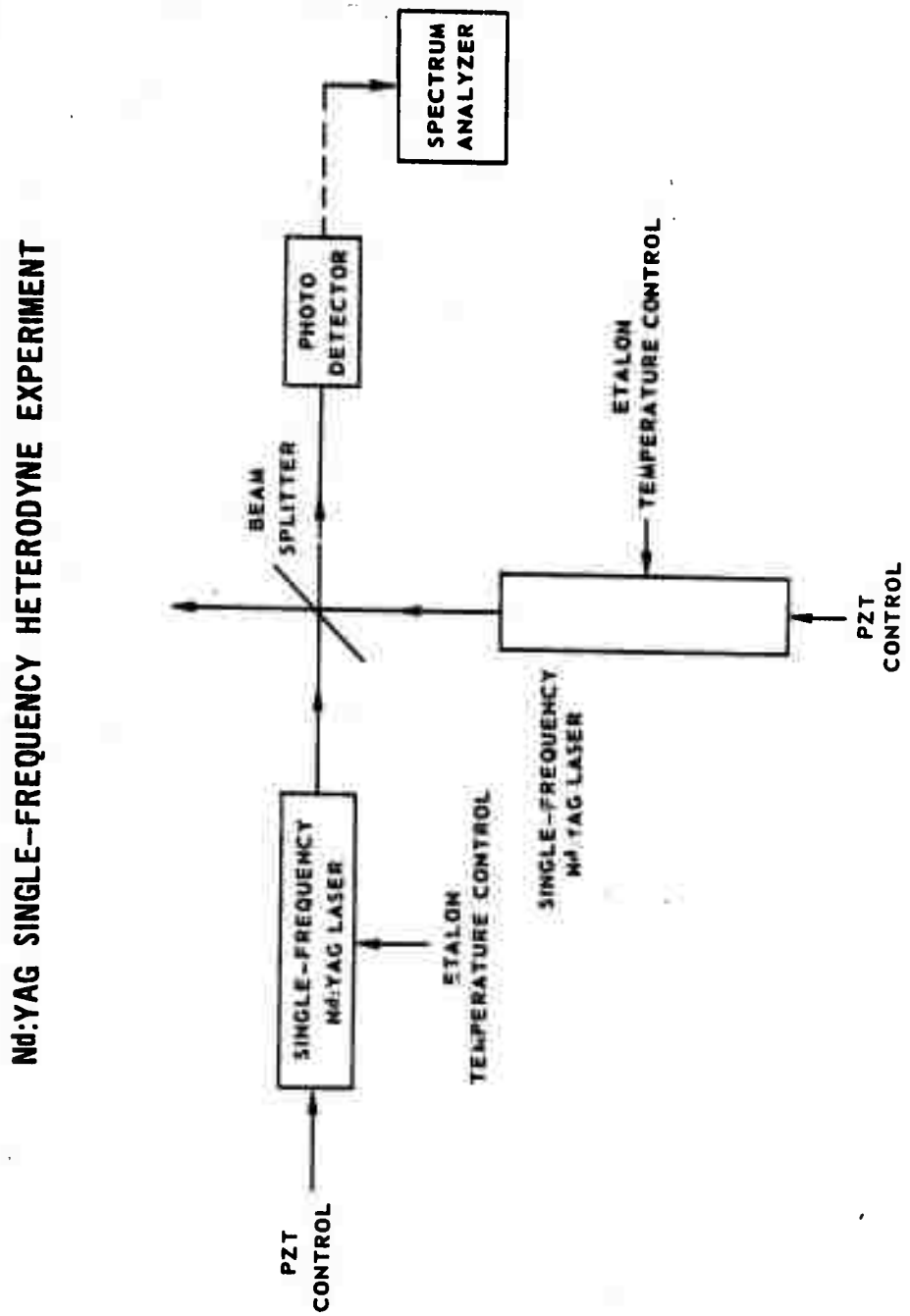
Nd:YAG SINGLE-FREQUENCY HETERODYNE EXPERIMENT
SPECTRUM ANALYZER
PHOTO DETECTOR
BEAM SPLITTER
ETALON TEMPERATURE CONTROL
PZT CONTROL
SINGLE-FREQUENCY Nd:YAG LASER
ETALON TEMPERATURE CONTROL
SINGLE-FREQUENCY Nd:YAG LASER
PZT CONTROL

HETERODYNED SIGNAL FROM TWO SINGLE-FREQUENCY Nd:YAG LASERS

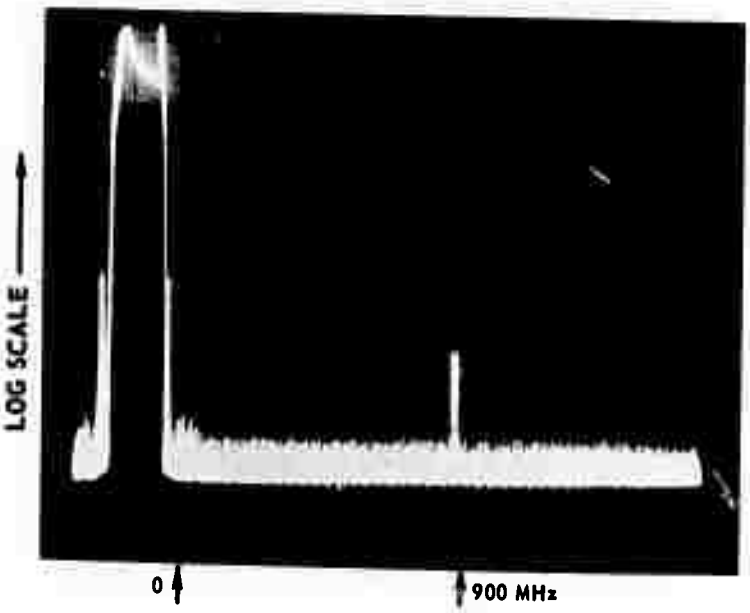

FREQUENCY, 200 MHz/div

III. DISCUSSION OF COHERENT IMAGING PROBLEMS

Synthetic Aperture Techniques

The section briefly reviews some of the basic principles involved in a coherent imaging radar (Refs.III-1 and 2).

In a conventional radar imaging system, the resolution is determined by the diffraction limit of the system, which, with an aperture D and a wavelength λ, is,

$$\Delta\theta = \lambda/D$$

So that the resolution at a distance R is

$$\Delta X = \lambda R/D$$

The maximum size of the aperture is determined by scintillations and angle of arrival fluctuations in the visible and infrared regions of the spectrum and in addition, in the microwave region, by fabrication problems. In the visible region, the largest useable aperture is of the order of 10 cm. At 10.6 μ it is approximately one meter*. Microwave apertures of tens to hundreds of meters or larger have been successfully operated. In the visible and IR regions then the minimum beam width is approximately 10^{-5} radians. Obtainable resolution is

R (km)	ΔX (meters)
1	.01
10	.1
100	1
200	2
1000	10
3×10^4	300
5×10^5	5×10^3 (moon).

Setting aside considerations of detectability for the moment, obtaining an image of an object of a few meters in size at a distance of 100-500 km is on the far edge of the capability of a conventional imaging system. Simple range gating using short pulses or duration τ can provide down-range resolution of the order of $\tau c/2$, independent of range. Nanosecond pulses can thus provide resolution of the order of 15 cm and shorter pulses correspondingly better resolution. If periodic trains of pulses can be processed coherently, then comparable or better cross range resolution on moving targets can be obtained from doppler information.

---

*The coherence area actually increaes as $\lambda^{6/5}$ and depends on the state of turbulence of the atmosphere. The values used here are quite optimistic. See, for example, Ref. 4, pp 128-144.

Coherent synthetic aperture techniques can be used whenever there is relative motion between the radar and the target. Two cases are usually considered, the rotating body range-doppler imaging used in radar astronomy and the side-looking radar used for terrain mapping. Fig. III-1a shows the geometry for a rotating sphere and FigIII-1b for a rotating cylinder. Range gating provides resolution in the down range direction, and doppler processing provides the resolution in the cross range direction. In the simple case of the rotating sphere, the contours of constant velocity are parallel to the axis of rotation as shown and together with the contours of constant range, provide a coordinate system on the target. The doppler shift is given by

$$\omega_d = 2\frac{\omega v}{c} = 2\frac{\omega \Omega x}{c}$$

where Ω is the rotation rate of the target, and x is distance from the axis of rotation.

The resolution in x will depend on how well we can resolve the doppler frequency, i.e.,

$$\Delta x = \frac{c}{2\omega\Omega}\ \Delta\omega_{dr}$$

where $\Delta\omega_{dr}$ is the doppler frequency resolution limit. If we observe the target for a time T, then $\Delta\omega_{dr} \approx 2\pi/T$ and

$$\Delta x = \frac{2\pi C}{2\omega\ \Omega T} = \frac{\lambda}{2\Omega T} = \frac{\lambda}{2\Delta\theta}$$

where $\Delta\theta$ is the angle through which the target has tuned during the observation time T. The cross range resolution can be very good at optical wavelengths. There is, of course, the problem of movement of features through the resolution elements during the observation time. There are techniques to handle this. We can estimate the magnitude of this effect. The x or cross range position of a given feature will change by $\delta x = R\Delta\theta$ during the observation time, and if it is not to move out of a range resolution cell

$$\delta x = R\ \Delta\ \theta < \Delta x = \frac{\lambda}{2\Delta\theta}$$

or

$$R\ \Delta\ \theta\ \Delta\ x < \Delta\ x^2$$

$$\frac{R\ \lambda}{2} < \Delta x^2$$

So that if $\lambda = 10\ \mu$ R = 10 meters

$$\Delta x^2 > \frac{10^{-5} \cdot 10}{2}$$

$$\Delta x > \frac{1}{\sqrt{2}} 10^{-2} \text{ meters}$$

i.e., as long as we do not try to resolve better than about 1 cm. The motion of features through doppler resolution lines will not be a great problem.

The other commonly discussed case of synthetic aperture imaging is in the side-looking radar case as shown in FigIII-2. Here the contours of constant doppler shift are the lines of constant azimuth. The doppler shift is

$$\omega_c = 2 \frac{\omega V}{c} \sin \theta \approx 2 \frac{\omega V}{c} \theta \text{ for small } \theta$$

In this case the maximum observation time is determined by the time the target is in the beam. If the beam width is

$$\delta\theta = \frac{\lambda}{D}$$

then the extent of the beam at a distance R is

$$\delta\theta\ R = \frac{\lambda R}{D}$$

and the target will move out of the beam in a time

$$T = \frac{\lambda R}{Dv}$$

So that the frequency resolution $\Delta \omega_{dr}$ is

$$\Delta \omega_{dr} = \frac{2\pi Dv}{\lambda R}$$

the resolvable angle is thus

$$\Delta \theta = \frac{c}{2\omega v} \Delta \omega_{dr}$$

$$= \frac{2\pi Dv}{\lambda R} \cdot \frac{c}{\omega v} = \frac{D}{2R}$$

and the resolvable cross range coordinate is $\Delta\theta R = \Delta x = D/2$. The apparently contradictory result, that the resolution improves as the aperture gets smaller, is simply a result of the fact that the time during which the target is illuminated, and hence, the maximum processing time, increases as the beam gets broader. Clearly, there is no advantage to be gained by reducing the aperture to dimensions smaller than a wavelength, since at this point the radiation pattern becomes nearly isotropic and no further increase in the processing time is possible. This also results in a large reduction in the power delivered to the target.

In the side-looking radar configuration just discussed, it is clearly immaterial whether the radar or the target is moving; it is only the relative motion that is important. Another interesting configuration that can be considered is one that is set-up to obtain an image of an extended target that is moving past the radar. In this case, the field of view of the radar need not remain fixed, but can be scanned to keep the target continuously in view. Consider the geometry shown in Fig III-3. For simplicity we will assume that the aperture is a phased array of only two elements and that the beam is scanned by means of the time-varying phase shifts ϕ_1 and ϕ_2. It may be readily shown that the signal received by this time-varying phased array from a point target at a point R_1 is

$$S = e^{i\omega t}\, e^{2ikR_1}$$

if one of the phases, ϕ_1 in this case, is set equal to zero.

We now want to calculate the spatial resolution that can be achieved by doppler processing the signal received from an extended target. Consider the geometry shown in Fig III-4, where the extended target is represented by two point targets. The behavior of the doppler shifts from the two targets is shown as a function of time and it has also been assumed that the shifts are displaced from zero by some offset frequency ω_{if}. Suppose now that the receiver is programmed to track the doppler shift from one of the targets. The differential doppler shift from the other will then be as shown in Fig III-5a. The differential shift is zero when both targets are far from the transmitter and the shift increases to nearly a constant value as the targets pass the antenna. The time during which the shift is appreciable is of the order of

$$T = \frac{2Z}{v}$$

and its magnitude is

$$\omega_d \approx \frac{\omega v}{c}\,\frac{\Delta x}{z}$$

The resolution that can be achieved in T is $\Delta\,\omega_{dr} \approx \frac{2\pi v}{2Z}$ so that the spatial resolution is

$$\frac{\Delta x \omega v}{cZ} \approx \frac{2\pi v}{2Z} \quad \Delta x = \frac{\lambda}{2}$$

independent of range, and aperture size. This result should not really be too surprising. In compensating for the doppler shift of one of the scattering centers, we have in effect cancelled its motion. The apparent motion of the other scattering center is then a rotation about the first (see FigIII-5b). In the observation time T, the combined object is viewed over an aspect angle $\Delta\theta = \pi/2$. If the object were simply rotating in the fixed field of view of the radar, we would expect to be able to resolve $\Delta x = \lambda/2\Delta\theta$ which is essentially the resolution that has been achieved. It is also the resolution that would be achieved by the non-scattering antenna if the aperture size were reduced to λ, but the loss of power has been avoided.

Signal Processing

The basic operation required of the processor for a synthetic aperture imaging system is the storage of the return over the processing time and the sorting of the received power into the appropriate range and doppler bins. As discussed above, the return from a point scatter does not have a single doppler shift but rather a doppler history. In the side looking radar case, this doppler history is nearly a linear frequency sweep when the target is near broadside. In the case of a point scatterer on a rotating body the doppler history is a sinusoidal function of time with a maximum as the point appears around the approaching edge, going to zero as the point passes the subradar point and reaching a maximum value but with opposite sign as the object disappears around the receding edge. The processing of this information would be a formidable task indeed, if it were not for the availability of coherent optical processing techniques. These techniques allow the parallel processing of the many range-doppler components of the received signal.

The use of optical techniques for processing of coherent microwave radar data has been highly developed (Ref. III-1 and 2). The basic ideas are illustrated in Fig. III-6-8. A train of short radar pulses having a carrier frequency ω_o as shown in Fig. III-6a is transmitted. The return signal, Fig. III-6b will have a duration $\tau = \frac{2\Delta R}{c}$ where ΔR is the range extent of the target. At each range, the motion of a scattering center will impose a doppler shift on the signal. Since the pulsed duration will typically be shorter than the reciprocal of the doppler frequency, this will manifest itself as a change in phase as a function of range. This phase may be obtained directly by heterodyning the received signal against a stable local oscillator, obtaining the signal shown in Fig. III-6c. This signal is the real (or imaginary) part of the complex amplitude of the radar return as a function of range. To obtain the doppler distribution and scattering intensity at a given range, we must follow the history of the signal at that range from pulse to pulse; i.e., one must perform a frequency analysis of the sampled data obtained from each range element.

This complicated signal processing operation can be accomplished readily with the system shown in Fig. III-7. The demodulated signal, together with a bias, is used to intensity modulate the trace of a CRT. The sweep is initiated at the start of the radar return and lasts for the duration of the return. The intensity modulated signal is recorded on film. When the next return is received, the film is moved horizontally and the return is recorded similarly. The result is a series of vertical strip records, with the vertical axis corresponding to range resolution within a single return and the horizontal axis corresponding to the pulse-to-pulse history of the amplitude and phase of the return at a given range.

Once the signal is recorded in this format, the signal processing can be performed very conveniently by optical techniques. Consider as an example, the side looking radar case. As the radar passes a point scatterer at a given transverse range, the return signal will be approximately a linear frequency sweep

$$A_{cos}\ (\omega_o t + \beta t^2)$$

after demodulating, and adding the bias term B, this signal becomes

$$A_{cos}\ (\omega_1 t + \beta t^2) + B$$

Here ω is the difference between the center frequency of the pulses and the reference local oscillator. In practice this is usually non-zero for reasons which will become clear later. By virtue of the film transport, the transparency then has a spatial dependence of

$$T(x) = A_{cos}\ (k x + \gamma x^2) + B$$

where $k = \omega_1/v$ and $\gamma = \beta/v^2$ with v the velocity of the film. The appearance of the film record for two targets at different ranges would be as shown in Fig III-7b. (The spatial carrier, kx, has been suppressed for ease of illustration). The record for each target can be considered as a Fresnel zone plate. If the film transparency is illuminated with coherent light, each of the elementary zone plates will bring the beam to a focus at a range corresponding to the (scaled) range of the original scatterer as shown in Fig III-7c. The plane of the images will be inclined as shown in the figure. In addition, the range information which was well resolved in the film plane will be degraded by diffraction. This can be corrected by the optical system shown in Fig III-8a. The conical lenselement is a cylindrical lens whose focal length is a function of range (vertical axis of film). This removes the tilt of the image plane of Fig III-7c and, with appropriate choice of focal length, moves the focal plane for the horizontal data record (aximuth history) to infinity. The cylindrical lens does the same for the vertical (range) data record. The final spherical lens brings both foci from infinity to the film plane. Fig III-8b shows a top view of the system and illustrates the offset angle due to the spatial carrier mentioned earlier. This is employed to displace the image from the light due to the bias term. The final focused image is recorded through an appropriately placed slit, each slit record being a record of the return for all ranges at a given azimuth.

Range and Doppler Spreads

The first consideration in the coherent optical imaging radar is the estimation of the magnitude of the return. The radar equation gives

$$\frac{Pr}{Pt} = 4\pi \underbrace{\left(\frac{D}{\lambda}\right)^2 \cdot \frac{1}{4\pi R^2}}_{\text{Incident Power Density}} \cdot \underbrace{\sigma \cdot \frac{D^2}{4\pi R^2}}_{\text{Cross Section}}$$

In the case where the target is just large enough to intercept the engire beam and scatters it isotropically, with unit reflectivity, this reduces to:

$$\frac{Pr}{Pt} = \frac{D}{4\pi R^2} = 8 \times 10^{-2} \frac{D^2}{R^2}$$

So that the attenuation factor for the power returned from a just resolvable element is

R km	D = 10 cm (λ=1μ)	D = 1 meter (λ=10μ)
1	8×10^{-10}	8×10^{-8}
10	8×10^{-12}	8×10^{-10}
100	8×10^{-14}	8×10^{-12}
1000	8×10^{-16}	8×10^{-14}
5×10^5	3.2×10^{-21}	3.2×10^{-19}

The next important consideration is the magnitude of the doppler shift and spread to be expected. The doppler shift is

$$fd = 1 \text{ MHz/meter/sec at } 1.06\ \mu$$

$$= 100 \text{ KHz/meter/sec at } 10.6\ \mu$$

For a rotating body, the doppler spread becomes

$$\Delta f \approx \pm 2\pi \text{ MHz/meter/rps at } 1.06\mu$$

$$= \pm .1 \times 2\pi \text{ MHz/meter/rps at } 10.6\mu$$

where the length scale is the characteristic dimension of the object normal to both its axis of rotation and the direction of illumination.

The case of a transiting satellite is illustrated in FigIII-9 for a wavelength of 10.6 microns. The doppler spread for a rotating body can be seen to be quite large and the average doppler shift for the transiting body is extremely large. Initially it would seem that a large doppler spread would require a receiver with a wide bandwidth and consequently a poor detection sensitivity. It should be kept in mind, however, that the information bandwidth of the system is not determined by the doppler shift. Given complete flexibility in the design of the transmitted waveform and the receiver, it can be shown that the ultimate detection sensitivity is not dependent on the absolute magnitude of the doppler shift or spread. The information that is desired is an image of the target so that the desired information channel capacity is determined by

$$C \approx \frac{NG}{T} \quad \text{bits/sec}$$

where N is the number of resolvable elements on the target, G the number of bits characterizing the strength of the signal from each resolvable element (gray scale) and T the total observation time.

Another important consideration is the so called spread factor of the target, i.e., the product of the doppler spread and the time delay spread. If we interrogate the target with a repetitive train of pulses having a separation T, then range ambiguities will be eliminated if

$$T > \frac{2\,\Delta R}{c} = \Delta\tau$$

where ΔR is the range spread. Doppler ambiguities will be avoided if the sampling rate $1/T$ is greater than twice the maximum doppler shift to be measured, so

$$\frac{1}{T} > 2\,\Delta f$$

Both can be simultaneously satisfied if

$$\Delta\tau\,\Delta f \ll 1$$

in which case the target is said to be underspread. For a rotating target, $\Delta f \approx \Omega\,\Delta R\, f/c$

$$\Delta\tau\,\Delta f \approx 2\Delta R^2\,\frac{\Omega f}{c^2} = 2\,\frac{\Delta R^2}{\lambda c}\,\Omega$$

At a wavelength of 1 micron, a 1 meter target becomes overspread at $\Omega \approx 1.5 \times 10^2$ radian/sec and at 10 microns $\Omega = 1.5 \times 10^3$ radians/sec. In all that follows, it will be assumed that the target is underspread. In the case of an overspread target, the amount of information that can be obtained is greatly reduced.

Initial experimental investigations will be concerned only with underspread targets.

Signal Design

The problem of range and doppler ambiguities discussed above is present in any radar system that is designed to simultaneously measure range and doppler shift. Th considerations involved in the proper signal design are usually discussed in terms o radar ambiguity function (Ref III-3). This function is $\Psi = |\chi(\tau,f)|^2$ where

$$\chi(\tau,f) = \int_{-\infty}^{\infty} u(t)\, u^*(t+\tau)\, \exp(-i\,2\pi f\, t)\, dt$$

and where u(t) is the transmitted signal. The physical significance of the ambiguit function is that it represents the magnitude of the response of a matched filter to a waveform that is shifted in frequency by an amount of f and in time by an amount τ with respect to the waveform to which the filter is matched. Since the returns from the various resolution elements on a moving target are time and frequency shifted versions of the transmitted waveform, the ability to resolve elements will depend on how well the received signal can be distinguished from a time and frequenc shifted version of itself. To completely characterize the problem we must also specify the target scattering function $\sigma(\tau,f)$. This gives the distribution per unit frequency and per unit delay time of the power received from the target, i.e., it is the total cross section presented by all elements of the target having a specified delay τ and doppler shift f.

If we transmit a signal u(t) and receive with a filter matched to the transmitted signal but having a frequency offset f, then the output as a function of f an the delay will be given by

$$P(\tau,f) = \int_{-\infty}^{\infty} \Psi(\tau' - \tau,\ f' - f)\ \sigma(\tau',\ f')\, d\tau' df'$$

If Ψ has a peak at (0,0) and is very small elsewhere, then it will behave as a delta function and the output becomes a direct measure of the scattering function $\sigma(\tau,f)$ which gives the desired image.

The ambiguity function for a finite train of short pulses of individual duration T_1, spacing T_2 and total duration T_3 is illustrated schematically in Fig III-10. It consists of a large central peak and subsidiary peaks spaced at $\tau = \pm n\, T_2$ and $f = + \frac{mc}{T_2}$. The frequency width of the central peak is proportional to $T_3^{-1,2}$, the reciprocal of the total duration of the pulse train' the time width is determined by T_1, the individual pulse duration. If the scattering function were independent of time, then it could be probed with arbitrarily good resolution provided that the total range and doppler spread are small enough to present interference from the subsidiary peaks. If the peaks of the ambiguity function are very narrow compar

to the width of the scattering function, then the output of a matched filter reviever would be a replica of the target scattering function centered at each of the peaks of the ambiguity function. The condition that the replicas that are centered at adjacent peaks do not appreciably overlap is the same as the requirement that the target be underspread.

From these considerations, it is clear that a train of short pulses is a very good choice of signal for probing the scattering function of an underspread target. Other considerations, such as a peak power limitation, might dictate the choice of a different signal; however, the present discussion will be confined to the short pulse case.

Receiving Systems

To obtain an image of the target, any receiver must sort out the returned power into range and doppler bins corresponding to the resolution elements on the target. Several possible schemes can be considered (Refs. III-4, 5).

Direct Detection

In principle, the receiver shown in Fig III-11 can perform the necessary processing. The return signal is range gated by some fast shutter technique and each range sample is analyzed in frequency by a bank of narrow band optical filters. The signal in each range-doppler bin is then detected by a photodetector, and integrated over a time T. If we assume that the detector is limited only by quantum noise, a condition which will not be realized in a practical system, then the signal to noise ratio at the output will be

$$S/N = \eta \frac{P}{2h\nu B} = \eta \frac{P\,T}{2h\nu}$$

where P is the signal power received in a given range-doppler bin, and η is the detector quantum efficiency. The quantity PT is just the total energy received in the observation time T, so that the minimum detectable signal is of the order of one photon per resolution element. Clearly, the detection sensitivity of this system is completely independent of the magnitude of the doppler spread of the target. Aside from the difficulty involved in achieving quantum noise limited operation, such a receiver would require unrealizably narrow optical filters prior to the detector, so it is of little practical interest.

Sub-Carrier System

In this system, the entire spectrum of the optical signal is detected prior to any frequency filtering (see Fig III-12. In this case, all absolute optical phase information is lost. All doppler information, however, has not been lost. Consider the return from a train of pulses separated by a time T and incident upon a target moving with a velocity v toward the receiver. The return pulses will be separated by a time T

$$\left(\frac{2vT}{c}\right) = T\left[1 - \left(\frac{2v}{c}\right)\right]$$

or the repetition frequency f_r becomes

$$f_r \left(1 + \frac{2v}{c}\right).$$

Thus this system can observe the doppler shift on the pulse repetition rate rather than on the optical frequency itself. This system in effect substitutes a microwave wavelength characteristic of the pulse repetition rate for the optical wavelength This leads to a corresponding degradation of the doppler resolution although it preserves the directionality of the optical system. The resolution capabilities of this sytem are therefore degraded over those of the direct detection system but may be adequate for many purposes. A more detailed discussion of the possibilities of this system is presented in Section IV.

Heterodyne System

The heterodyne system shown in Fig.III-3 is capable of realizing the necessary doppler resolution. Heterodyning with a mode-locked laser (either with or without a frequency offset) provides the necessary range gating. The signal from each range element contains frequency components from all doppler elements in that range; generally, this will include nearly the entire doppler spread. The doppler shifts will be spread around the offset (IF) frequency. After the IF, the doppler bins can be resolved by a bank of parallel filters of bandwidth equal to the desired doppler resolution width. Following this resolution, the individual signals are square law or envelope detected and then smoothed over a time T. We may make some qualitative estimates of the signal to noise ratio for this receiver. Assuming that the local oscillator is strong enough so that its shot noise dominates the noise coming from the mixer, and assuming that the IF bandwidth B_{if} is twice the doppler spread, then the power signal to noise ratio at the output of the IF is given by

$$\frac{S}{N} = \frac{\eta P_o}{h\nu B_D}$$

where P_o is the total signal power from the range element, and B_D is the doppler spread. At the output of each of the doppler frequency filters the ratio is the same

$$S/N = \frac{\eta P_o\ (B/B_D)}{h\nu B} = \frac{\eta P_1}{h\nu B} = \frac{\eta P_o}{h\nu B_D}$$

where B is the bandwidth of the doppler bin and P_1 is the signal power in the range-doppler bin (assuming that it is uniformly distributed). The signal at this point is essentially noise-like and indistinguishable from the shot noise except by its amplitude. After the square law detector the signal to noise will be of the order of

$$\frac{S}{N} \sim \frac{1}{2}\ \frac{\eta P_1}{h\nu B}$$

Post detection integration can improve this. The number of independent samples taken in a time T is BT. The mean value increases as BT and the RMS fluctuations as $(BT)^{1/2}$. With an integration time T, then the S/N can be improved by a factor of $(BT)^{1/2}$ so

$$\left(\frac{S}{N}\right)_T \approx \frac{1}{2}\eta\frac{P_1}{h\nu}\left(\frac{T}{B}\right)^{1/2} = \frac{1}{2}\eta\frac{P_1T}{h\nu}\frac{1}{(BT)^{1/2}}$$

The quantity P_1T is the total number of photons received in the given range-doppler bin and is proportional to the total energy transmitted. Given the constraint of a fixed energy in the transmitted signal, the best S/N would be obtained by transmitting it all in a time T = 1/B and eliminating the post-detection integration completely. In this case

$$S/N \approx \frac{1}{2}\eta\frac{E}{h\nu}$$

so that the minimum detectable signal is of the order of one photon per range-doppler bin. If the constraint is a fixed peak power, then the signal to noise improves with post detection integration, but is never as good as coherent detection over the same time interval. The incoherent direct detection system, if it could be constructed and operated in the quantum noise limited region, would have approximately the same ultimate sensitivity but in that case the time duration of the transmission would be unimportant.

Energy Requirements

If complete flexibility in the design of the transmitter and receiver is assumed, then the ultimate sensitivity of a coherent optical imaging radar depends only on the energy received from the target. If we assume that a target whose scattering function is uniformily distributed in range and doppler shift is to be resolved into M resolution elements, the energy received in each will be

$$E = \frac{E_t L_p}{M}\rho$$

where E_t is the energy incident on the target, ρ is the effective reflectivity, and L_p is the propagation loss from the target to the detector. The signal to noise ratio for each resolution element would then be

$$(S/N) = 1/2\ \eta F\rho\ \frac{E_tL_p}{Mh\nu}$$

where F represents any additional system losses.

If we assume as before, that the entire target is just resolved, i.e., that it intercepts the entire beam, then E_t is just the transmitted energy. The transmitted energy required to obtain a given signal-to-noise ratio is then

$$E_t = 2 \frac{Mh\nu}{\eta F_\rho L_\rho} \quad (S/N)$$

As an example, let us assume $M = 10^2$ resolvable spots, $(S/N) = 10$, $\eta F_\rho = 10^{-2}$*, then for $\lambda = 10.6$ microns

$$E_t = 3.8 \times 10^{-15} L_p^{-1} \text{ joules}$$

and for $\lambda = 1.06$ microns

$$E_t = 3.8 \times 10^{-14} L_p^{-1} \text{ joules}$$

These energies are plotted in Fig. 14. The aperture sizes assumed in the figure are 10 cm for 1.06μ and 1 meter for 10.6μ. The differing aperture size accounts for a factor of 10^2 difference in the results for the two wavelengths and the reduced quantum noise at the larger wavelength for the remaining factor of 10. The energy required for the 10.6μ system is extremely modest, and ignoring other considerations, this would be the preferred wavelength of operation. Presently available CO_2 lasers have adequate coherence properties, but they lack the bandwidth to provide centimeter range resolution. The Nd:YAG laser, however, has both adequate bandwidth and coherence to obtain this type of resolution and initial experiments with this laser will be carried out.

* Assumes $\eta \approx .3$ characteristic of a PIN photodiode at 1.06 microns diffuse reflectivity .1 and other losses $\sim .33$.

Glint Points

In all the previous discussions, it has been assumed that the target is a perfectly diffuse reflector. This is very conservative and leads to a low estimate of the magnitude of the returned signal. An actual target will exhibit many glint points arising from smooth surface areas oriented perpendicular to the direction of illumination and having locally long radii of curvature. These glint points will lead to return signals that are orders of magnitude larger than the diffusely reflected signals that have been discussed.

Consider a diffusely reflecting area of diameter d located on a rotating target of diameter D_T. The power received by a receiver of aperture D_T, at a distance R, will be

$$P_r = P_i \frac{D_R^2}{4\pi R^2}$$

where P_i is the power incident on the area. Assuming as before that the entire target is just resolved, we have

$$D_T \approx \frac{\lambda R}{D_R}$$

and

$$P_r = P_i \frac{\lambda^2}{4\pi D_T^2}$$

as before.

We now consider the specular reflection from a smooth area of diameter d, oriented perpendicular to the illumination. This area will reflect power back in a solid angle

$$\Delta r \approx \left(\frac{\lambda}{d}\right)^2$$

instead of 4π so that

$$P_r = P_i \left(\frac{d}{\lambda}\right)^2 \frac{D_R^2}{R^2}$$

$$= P_i \left(\frac{d}{D_T}\right)^2$$

This simply reflects the gain $4\pi d^2/\lambda^2$ of the reflecting element over an isotropic scatterer. For d = 1 cm, $\lambda = 1.06\mu$, it amounts to $4\pi \times 10^8$.

We must now consider the fact that the target is rotating, so that the normal to the glint point area will not remain parallel to the illumination. This turns out not to be a problem. A glint point that is properly oriented to reflect specularly back to the receiver will remain properly oriented during the coherent integration time, in spite of the target rotation. This is easily shown. In the coherent integration time, the target rotates by an angle $\Delta\theta = \Omega T$, and hence, the normal to the glint point rotates by the same angle. If this angle of rotation is less than the beam width from the glint point, then the receiver aperture will remain illuminated by it during the integration time. This requires that

$$\Delta\theta < \frac{\lambda}{d}$$

We have found previously however, that the cross range resolutions Δx is given by

$$\Delta x = \frac{\lambda}{2\Delta\theta}$$

$$\Delta\theta = \frac{\lambda}{2\Delta X}$$

So we have

$$\frac{\lambda}{2\Delta x} < \frac{\lambda}{d}$$

$$d < 2\Delta x$$

So, that if the dimension of the glint point is less than twice the desired cross range resolution, the receiver aperture will remain illuminated by it during the entire coherent integration time.

In the above, we have assumed that the glint point was a planar surface. In practice, the points will arise from surfaces with long radii of curvature. This will reduce the gain of the glint over one isotropic scatterer and thus reduce the received power. The orientation requirement is more easily satisfied due to the increased beam width.

REFERENCES

III-1. Harger, R. O.: Synthetic Aperture Radar Systems, Academic Press, New York.

III-2. Notes Entitled, Principles or Imaging Radars, University of Michigan Engineering Summer Conferences, July 20-31, 1970, University of Michigan, Ann Arbor, Michigan.

III-3. Cook, C. E. and M. Bernfeld: Radar Signals, p. 59 ff, Academic Press, New York, 1967.

III-4. Pratt, W. K.: Laser Communication Systems, John Wiley and Sons, Inc., New York, 1969.

III-5. Ross, M.: Laser Receivers, John Wiley & Sons, Inc., New York, 1966.

ROTATING BODY RADAR

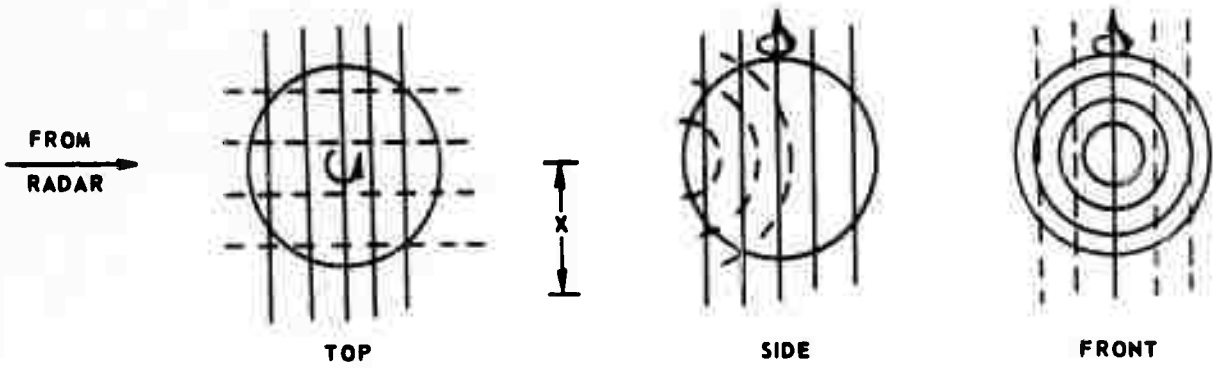

a) SPHERE

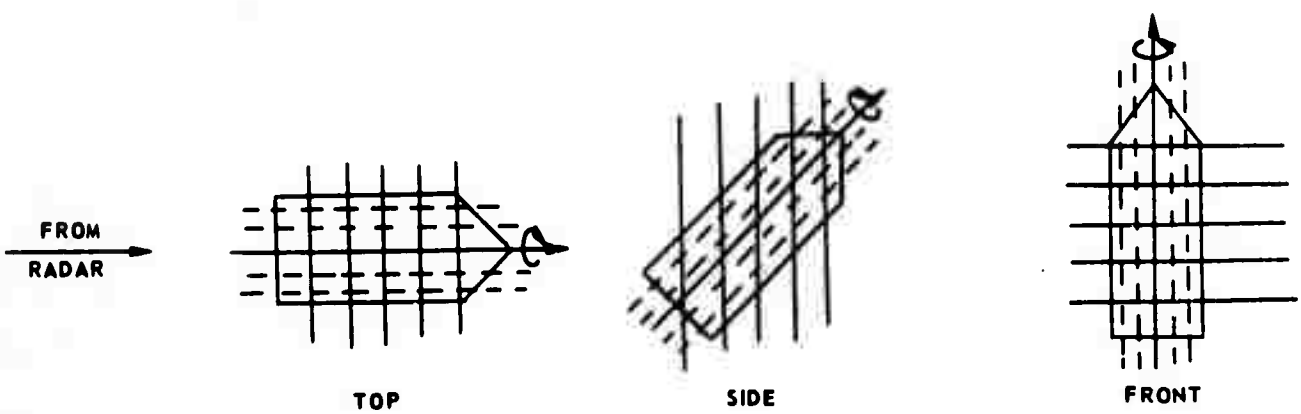

b) CYLINDER

FIG. III-2

SIDE LOOKING RADAR

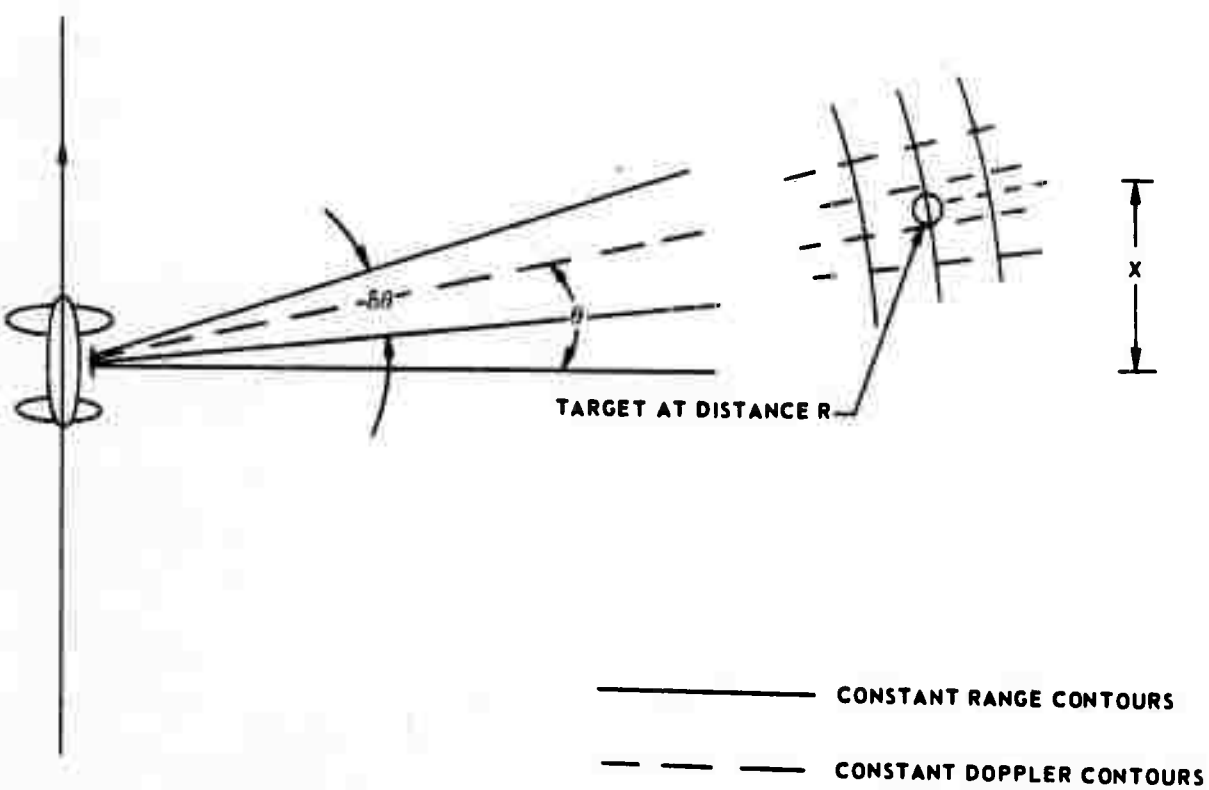

SCANNING SIDE LOOKING RADAR

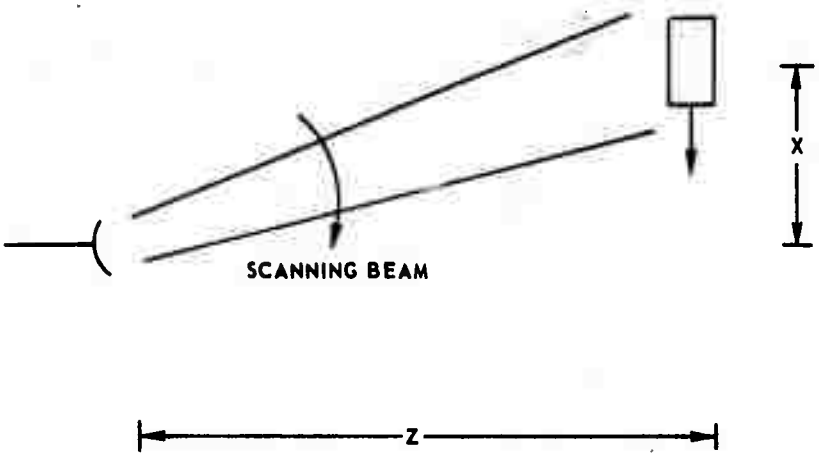

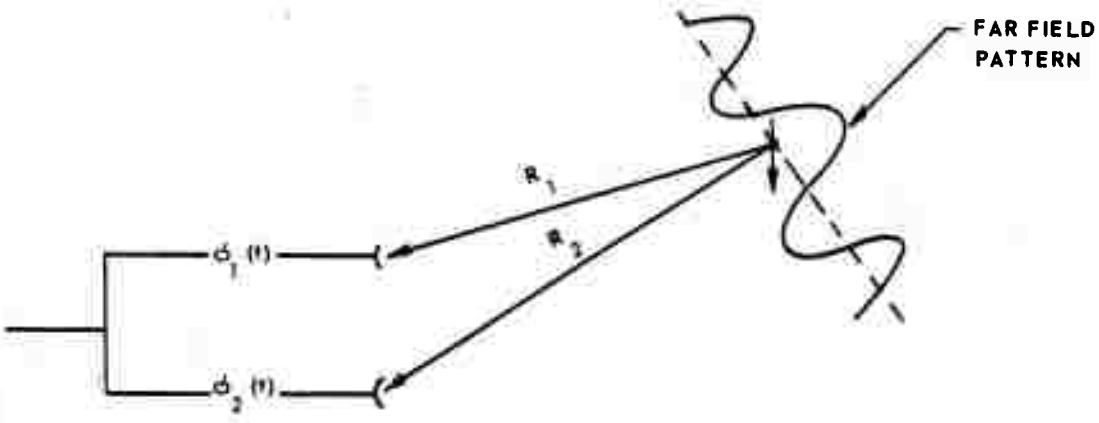

POINTING CONDITION

$$\phi_1 = \phi_2 + k(R_1 - R_2)$$

$$\phi_2 = k(R_1 - R_2) \text{ WITH } \phi_1 = 0$$

RESOLUTION OF SCANNING SYSTEM

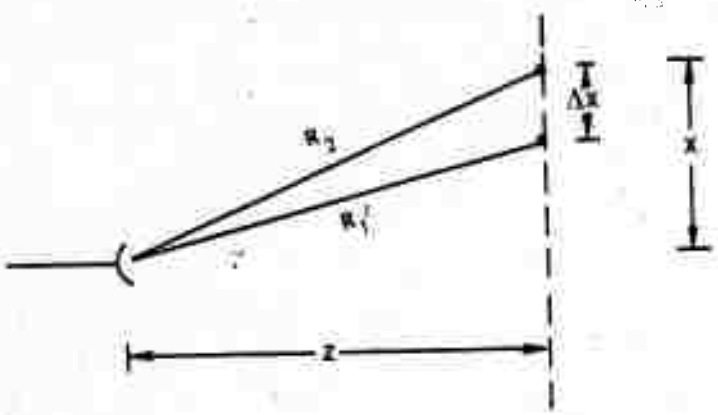

$$R_1 = \sqrt{Z^2 + X^2} = \sqrt{Z^2 + (vt)^2}$$

$$R_1' = \sqrt{Z^2 + (X-\Delta X)^2} = \sqrt{Z^2 + (vt-\Delta X)^2}$$

DOPPLER SHIFT

$$W_d = \frac{\partial}{\partial t} kR = \frac{W}{C} \frac{v^2 t}{\sqrt{Z^2 + (vt)^2}} = \frac{W}{C} v \frac{\ddot{x}}{\sqrt{Z^2 + X^2}}$$

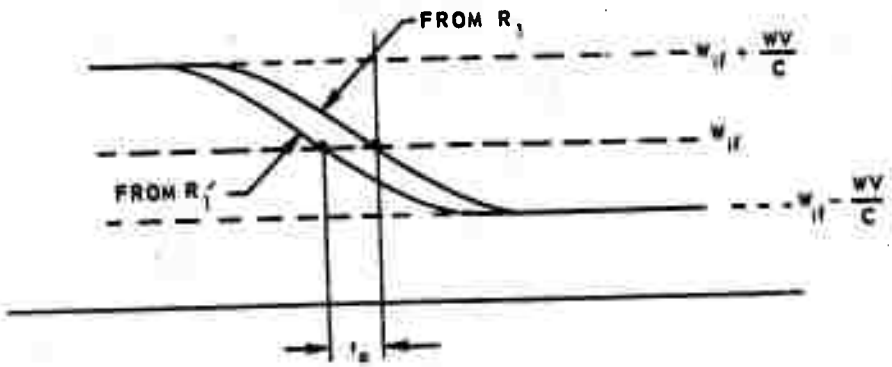

$$t_o = \frac{\Delta X}{v}$$

L920479-36

FIG. III -5

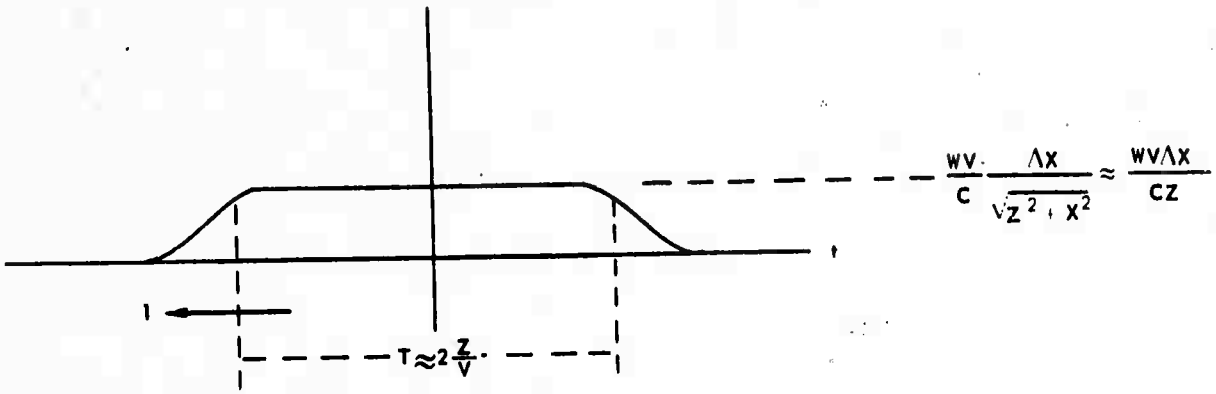

a) DIFFERENTIAL DOPPLER SHIFT

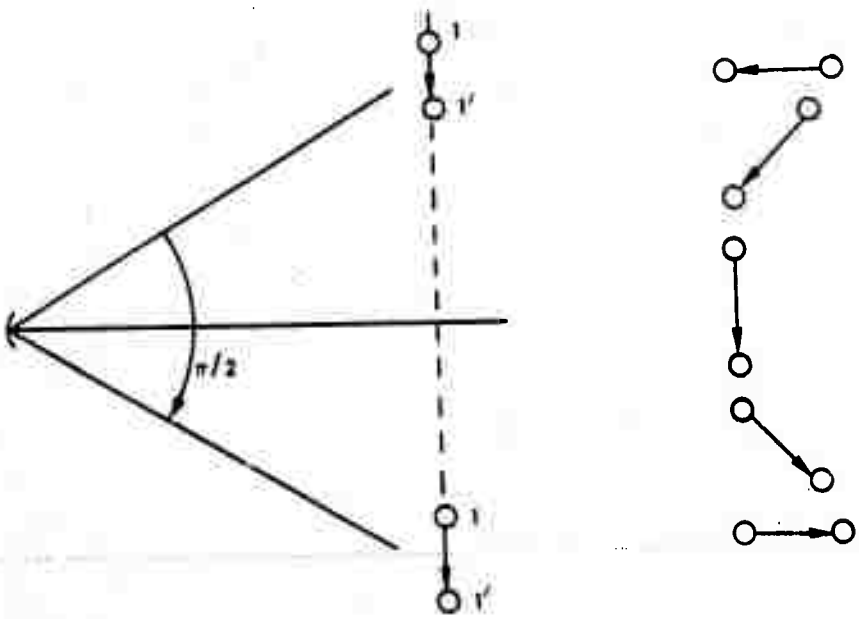

b) APPARENT MOTION OF SCATTERING CENTERS

FIG. III-6

SYNTHETIC APERTURE SIGNAL PROCESSING

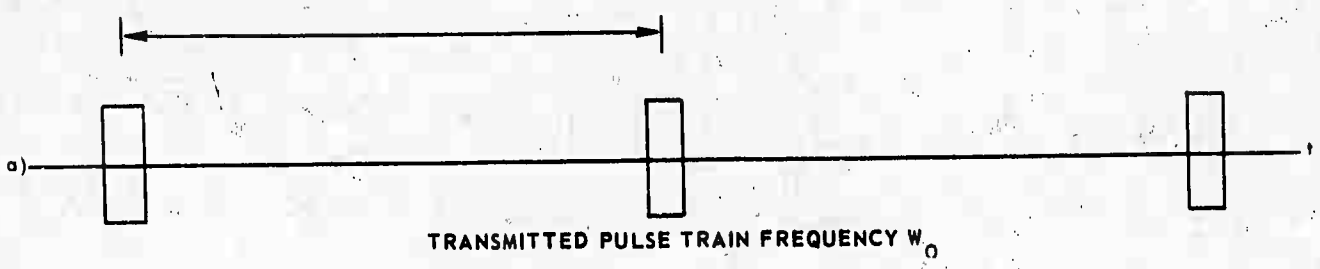

TRANSMITTED PULSE TRAIN FREQUENCY W_0

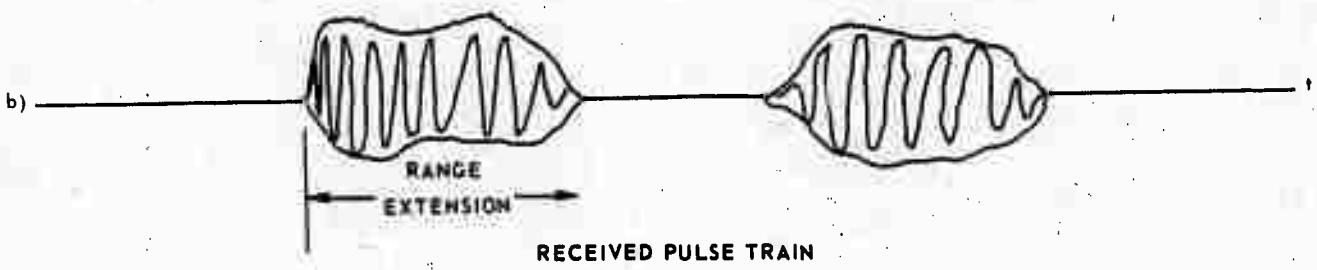

RECEIVED PULSE TRAIN

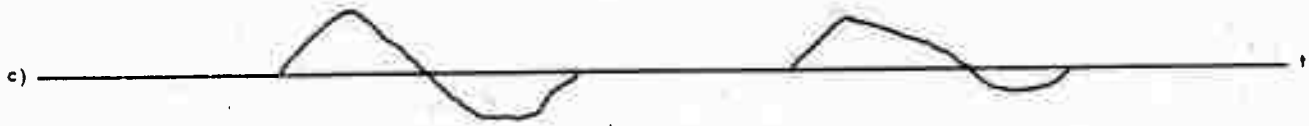

SIGNAL AFTER HETERODYNING WITH STABLE LOCAL LOAT W_0

EACH PULSE GIVES $I(r) \cos \phi (r)$

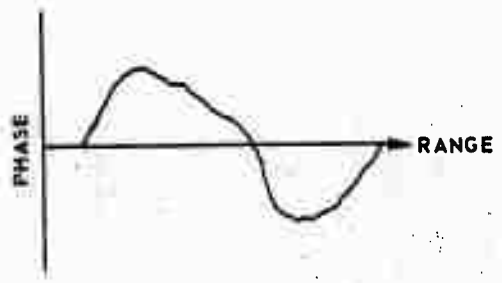

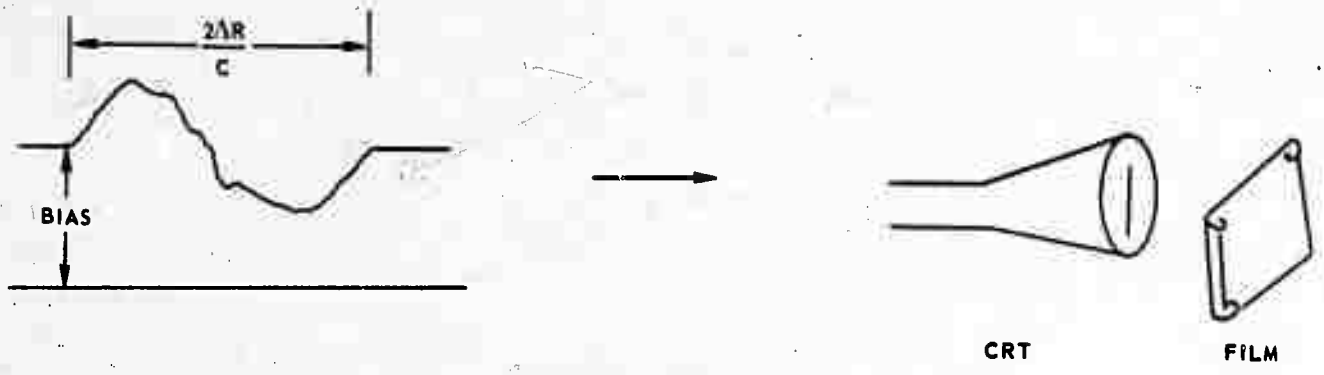

a) DEMODULATED SIGNAL

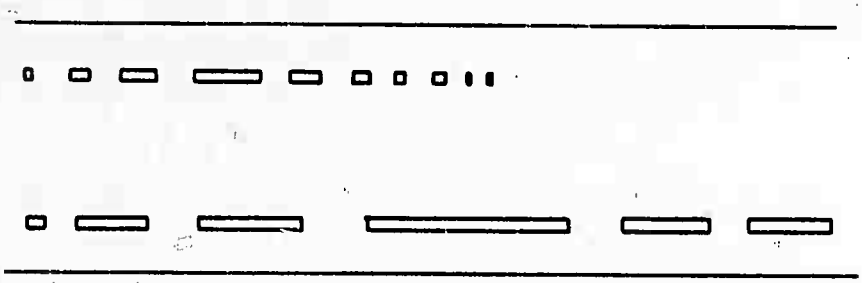

b) FILM RECORD

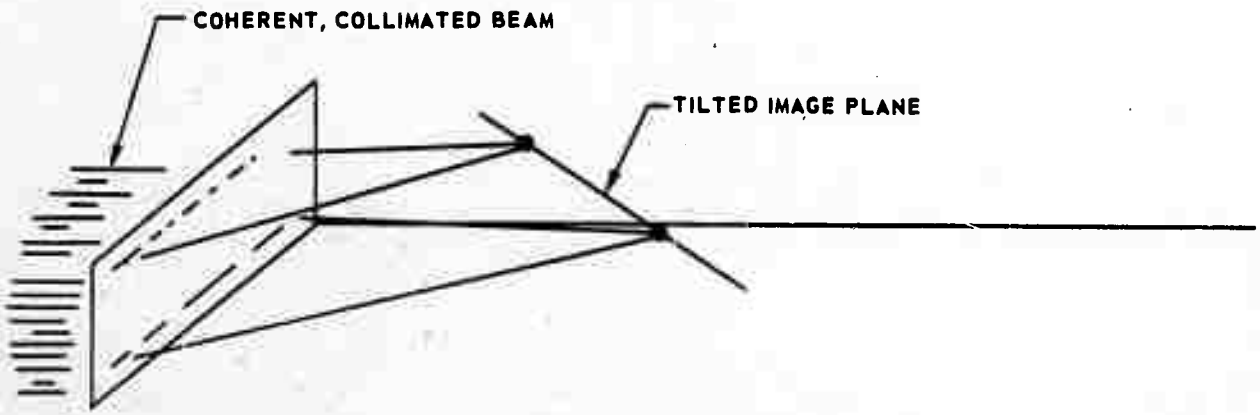

c) FOCUSING GEOMETRY

COHERENT OPTICAL PROCESSING SYSTEM

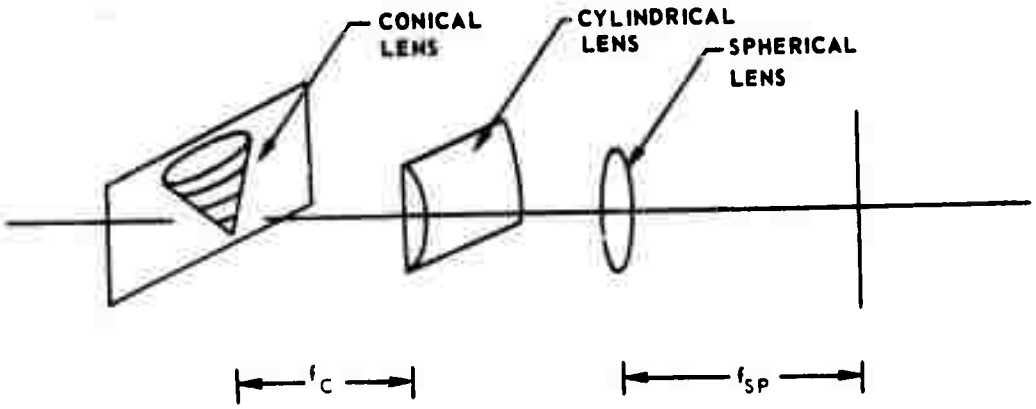

a)

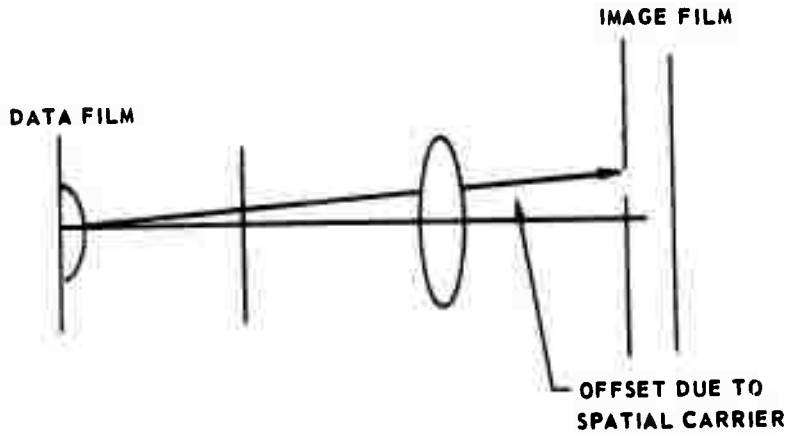

b)

VELOCITY AND DOPPLER FREQUENCY VARIATION

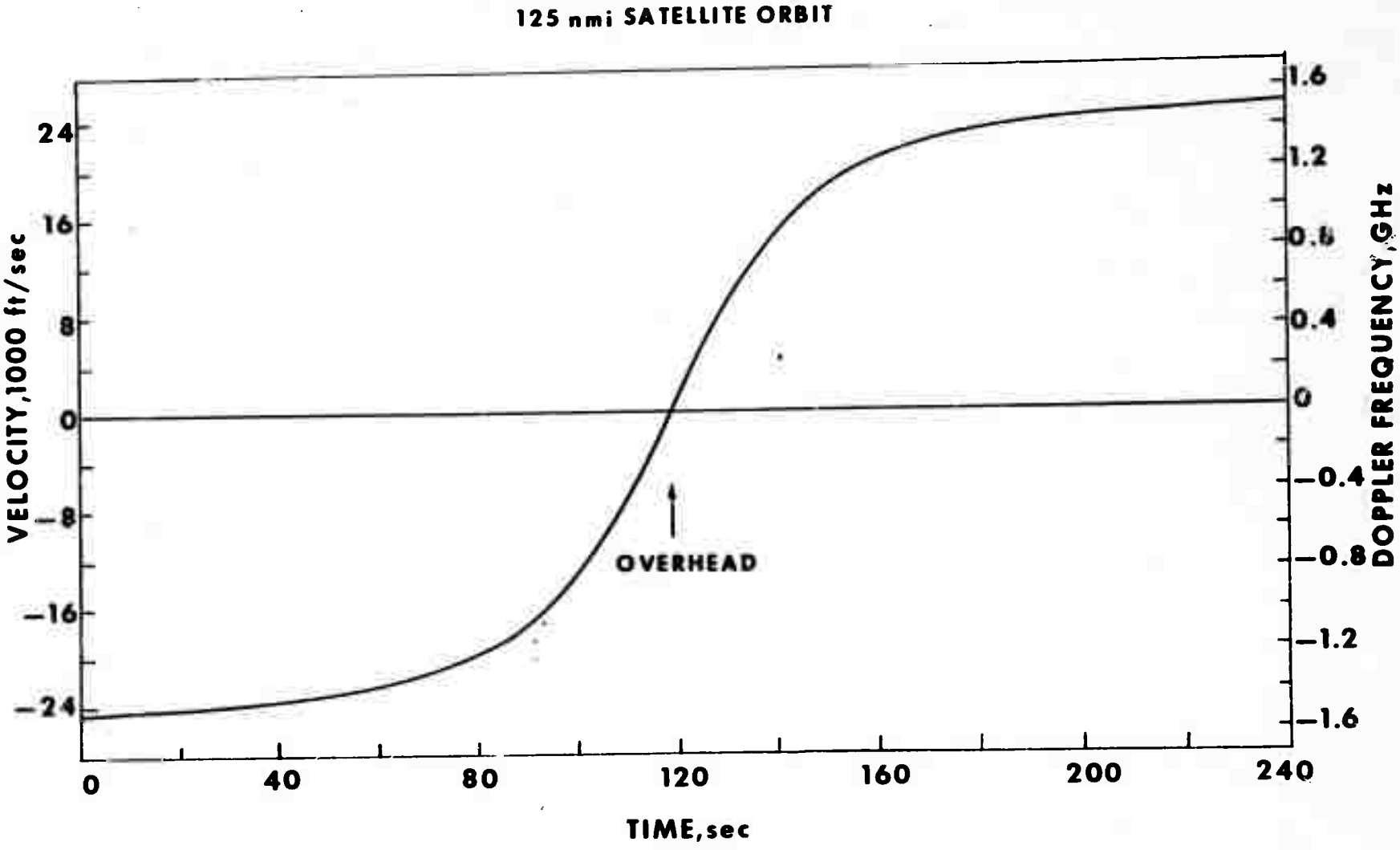

FIG. III-9

AMBIGUITY FUNCTION FOR MODE LOCKED PULSE TRAIN

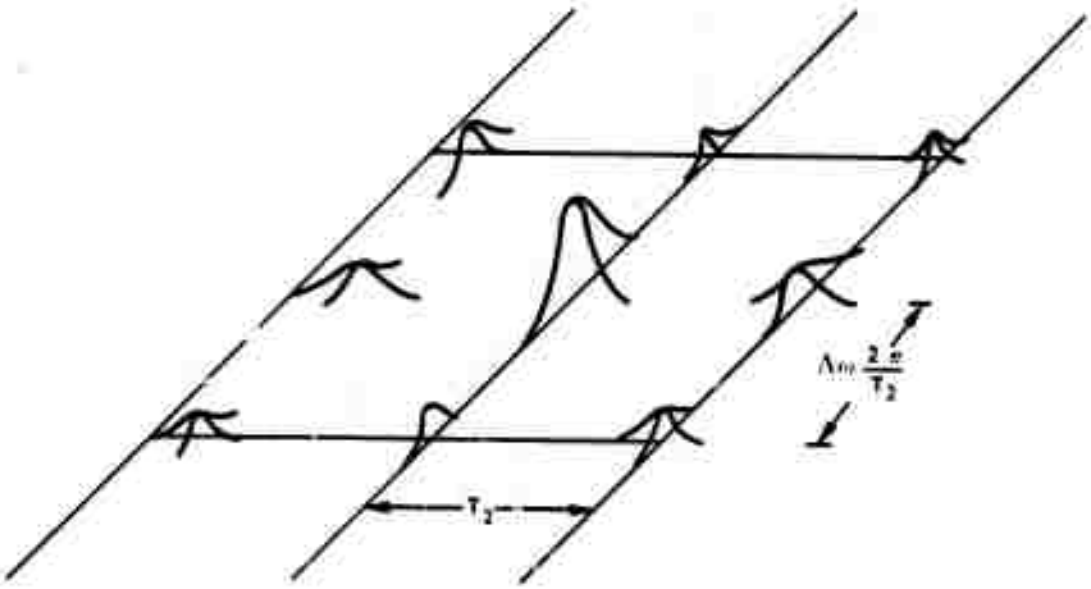

T_1 = PULSE WIDTH

T_2 = PULSE SEPARATION

T_3 = TOTAL DURATION OF PULSE TRAIN

CENTRAL PEAK

$\delta\omega \sim \frac{1}{T_3}$ $\quad$ $\delta T \sim T_1$

DIRECT DETECTOR

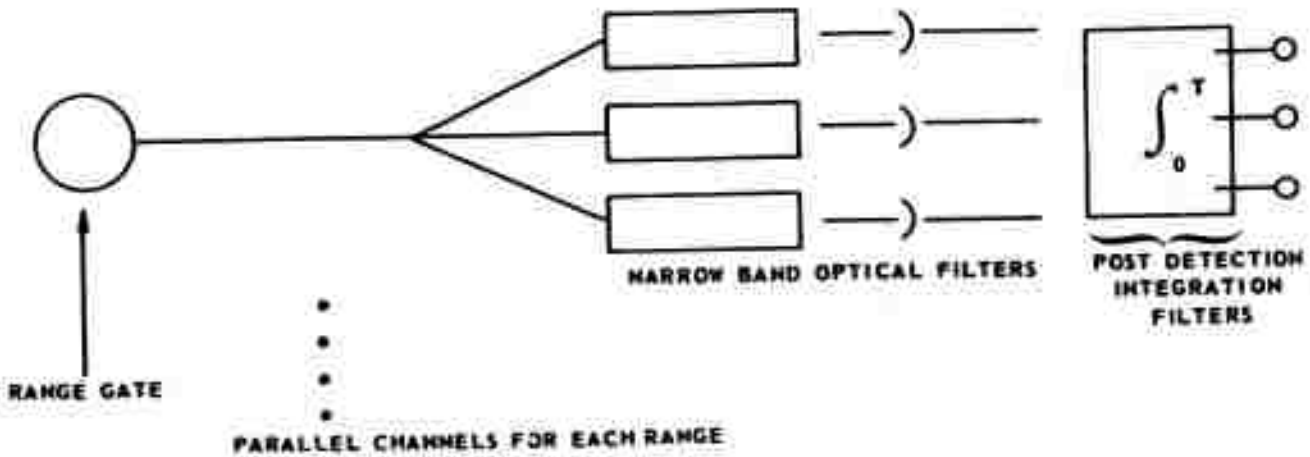

FIG. III-11

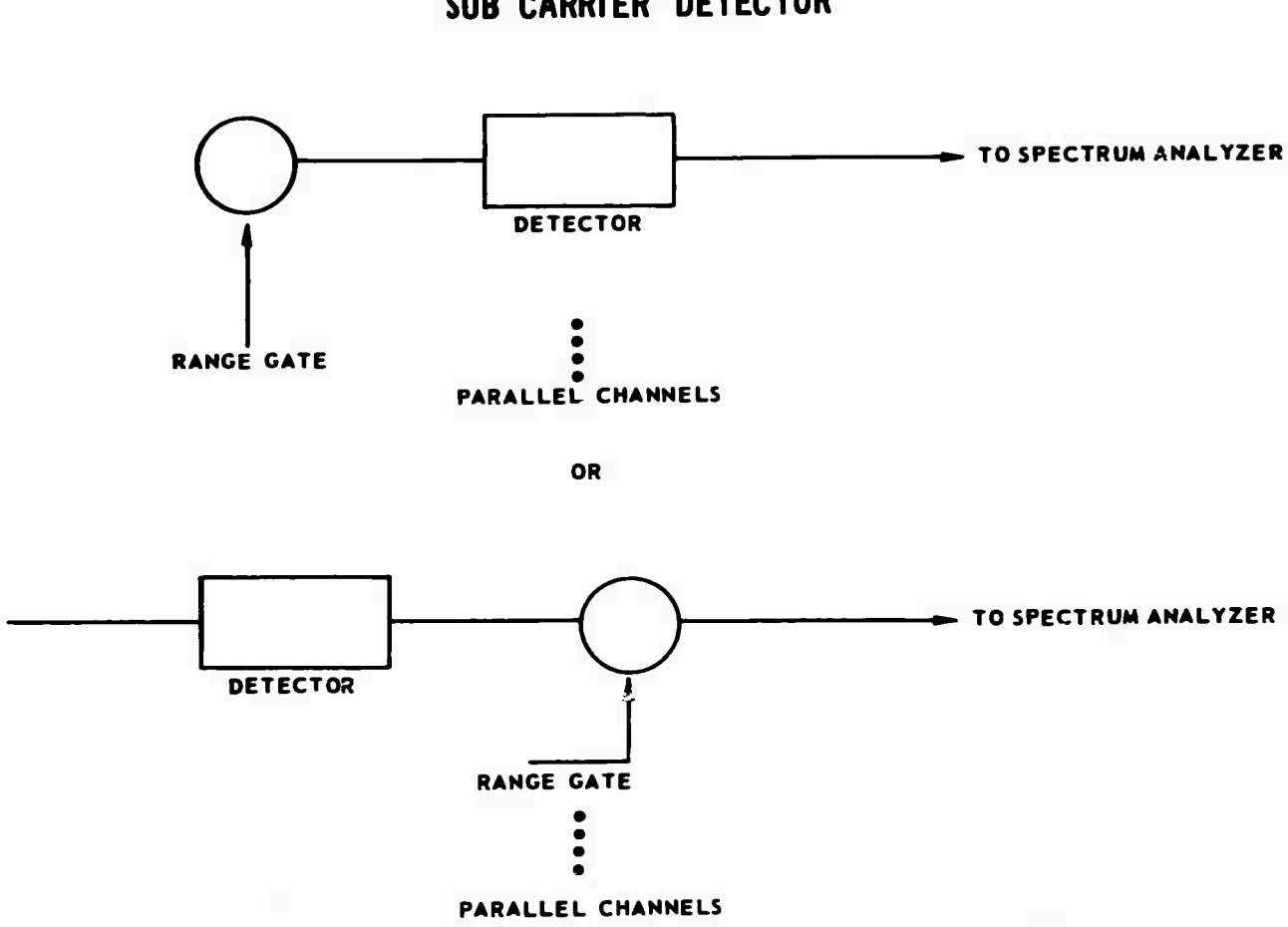
SUB CARRIER DETECTOR
TO SPECTRUM ANALYZER
DETECTOR
RANGE GATE
PARALLEL CHANNELS
OR
TO SPECTRUM ANALYZER
DETECTOR
RANGE GATE
PARALLEL CHANNELS

FIG. III-1

HETERODYNE DETECTION SYSTEM

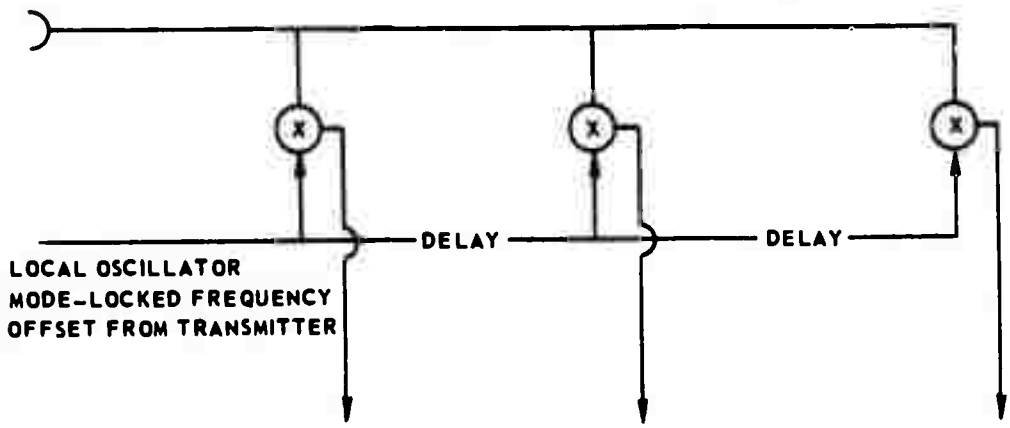

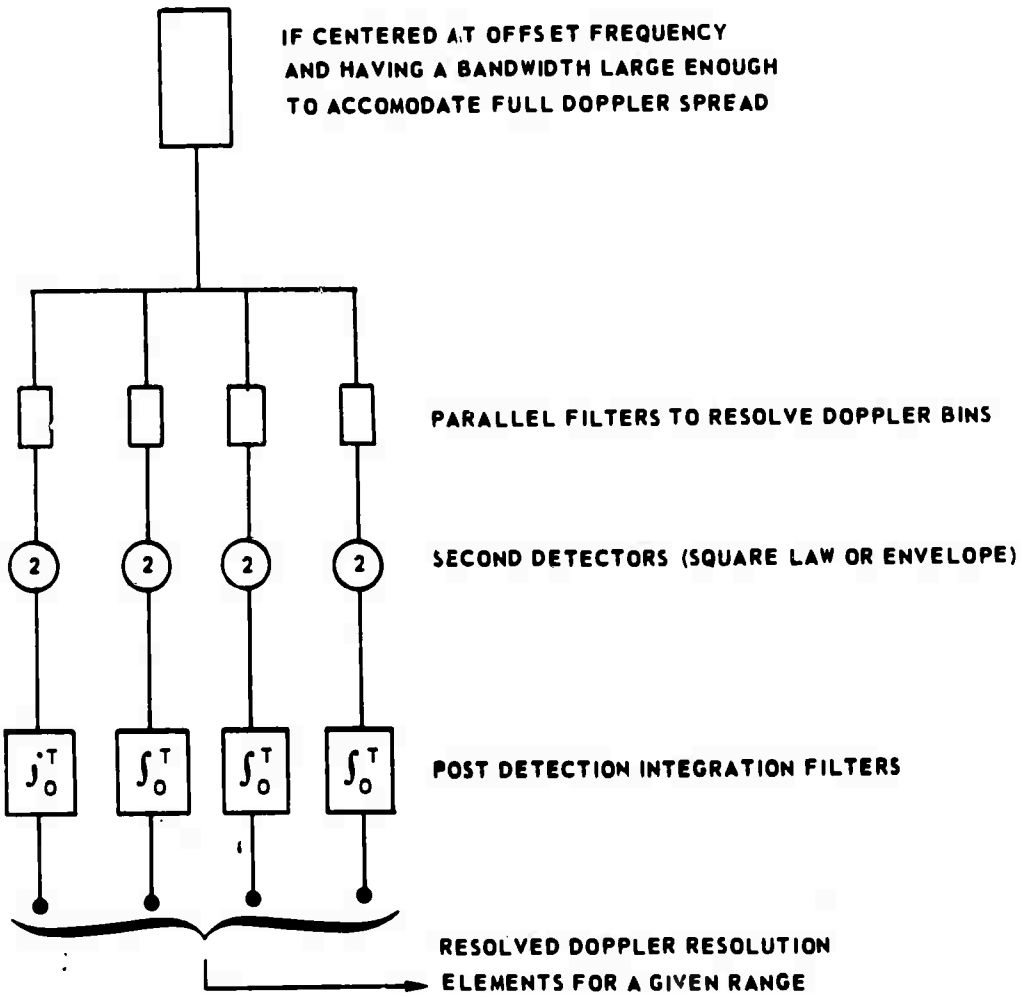

FIG. III-14

TRANSMITTER ENERGY REQUIREMENTS

$M = 10^2$ RESOLVABLE SPOTS

(S/N) = 10

$pnF = 10^{-2}$ (SYSTEM LOSS)

OPTIMUM SIGNAL & RECEIVER DESIGN

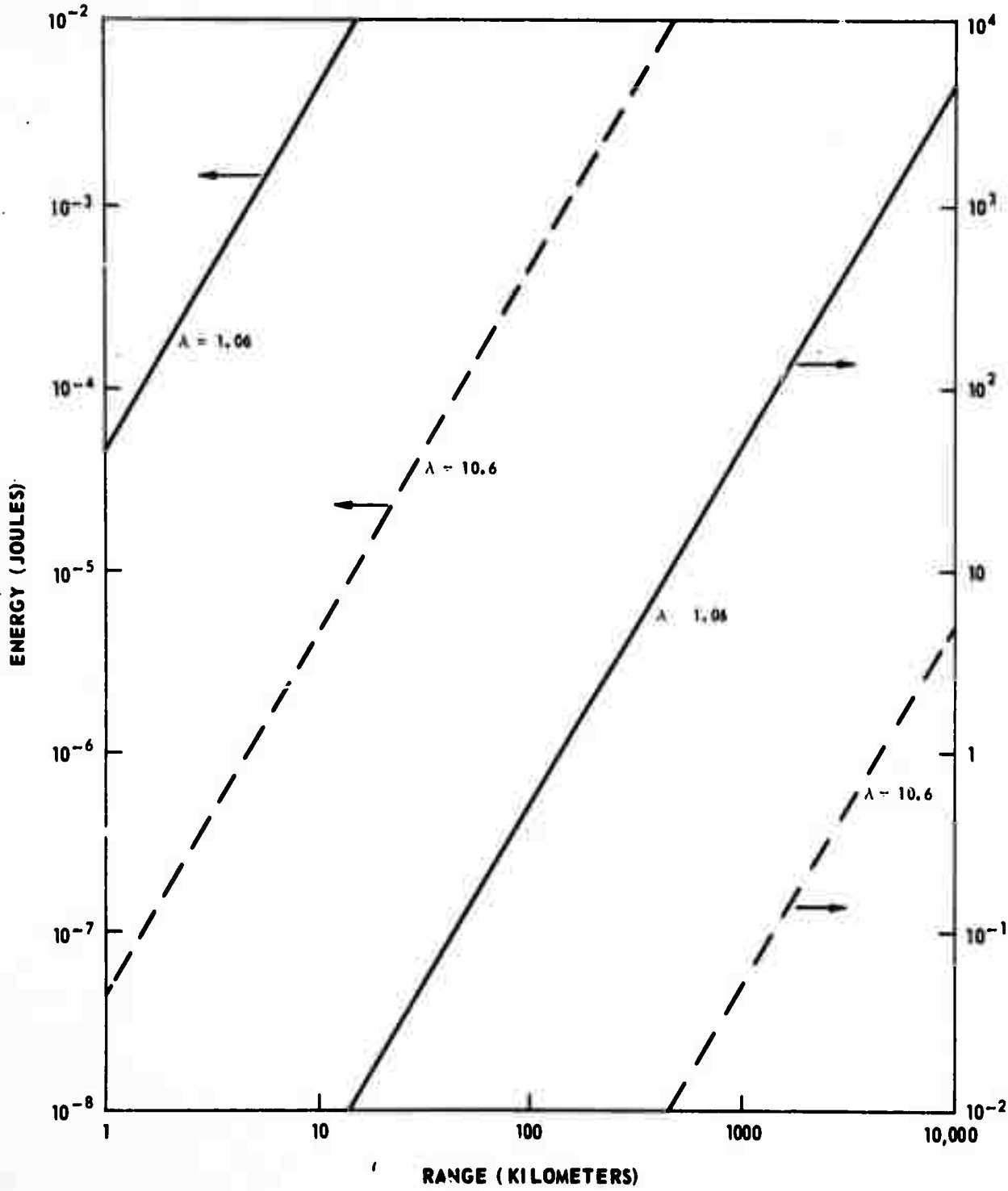

IV. LABORATORY INVESTIGATION OF COHERENT IMAGING TECHNIQUES

The object of this portion of the present contract and the anticipated amendment involves the investigation of the use of ultrashort pulses together with doppler processing to obtain high resolution imaging of moving laboratory targets.

The ideal laser source for this experiment would be a mode-locked laser that emitts a train of identical ultrashort pulses with highly reproducible characteristics over a time given by the reciprocal of the desired doppler resolution. The pulses should have the shortest possible duration, posses uniform phase fronts and be phase coherent from pulses to pulse.

In an operational system the coherence of the local oscillator used for heterodyning must be maintained over the round trip time of the signal from the target. Provisions must be made to compensate for the large doppler shift due to translation of the spinning target. Finally, sufficient power must be available to overcome the large propagation loss discussed in SectionIII, to ensure an adequate signal to noise ratio at the receiver. In a laboratory simulation, the coherence requirement may be easily met since propagation times are very small. Imaging of a purely rotating target eliminates the need for extremely large local oscillator offsets. The power requirements, however, are not reduced by the reduction in target range. This arises because of the spatial coherence requirements imposed by the optical heterodyne detector. If a distant target intercepts all of the power in the beam from the transmitter, and if it scatters the power uniformly in angle, then the power received by the receiver is just the solid angle subtended by the receiver aperture as viewed from the target. In the case where the target is just resolved, this will be of the order of

$$Pr = Po \frac{1}{4\pi} \left(\frac{\lambda}{d}\right)^2$$

where d is the target diameter. In the case of a target at very close range, essentially all of the power scattered back toward the receiver can be intercepted by the receiving aperture. Only a small fraction of this however is useful for the heterodyne detection. The angular coherence interval for power scattered from different point scatters on the target is approximately $\Delta\theta = \frac{\lambda}{d}$. The field of view of the receiver must be limited to this to avoid loss of signal. Again assuming isotropic scattering, the total useful received power is again of the order of $Po\ (\lambda/d)^2/4\pi$.

The problem of heterodyning from a diffusely reflecting target has been analyzed in more detail by Massey (Ref. IV-1). He considered the heterodyning of a signal reflected from a spot on a diffusely reflecting target. He considered the surface to be made up of a large number of scatteres of dimension small compared to a wavelength, and determined the optimum receiver field of view and the resulting IF current. For the case when the illuminated spot was not resolved by the receiver, he found

$$i_{iF} \approx \frac{D}{2R} \left(\frac{2I_{lo} P \rho \eta e}{h\nu} \right)^{1/2}$$

and for the case where the spot was resolved but the individual scatters were not,

$$i_{iF} \approx \frac{1.22\lambda}{d} \left(\frac{2I_{lo} P \rho \eta e}{h\nu} \right)^{1/2}$$

Here D is the receiver aperture, d the spot size, and P the power incident in the entire spot. In the case when the spot is just resolved corresponds to $1.22\lambda/D$ $R = \frac{d}{2}$. In this case, the expressions become identical and, subject to the resolution conditions, independent of range.

From the discussion in Section III, the power/energy requirements for an imaging system can be estimated. We assume for illustration, a laboratory target of diameter d = 10 cm, which is to be resolved into 100 resolvable elements (10 in range and 10 in doppler shift). We shall also assume that the signal processing will be done by transmitting a train of pulses of total duration equal to the reciprocal of the doppler resolution desired. The total energy received useful for heterodyning will then be

$$E_r \approx \frac{1}{4\pi} \left(\frac{\lambda}{d} \right)^2 E_t \approx 8 \times 10^{-12} E_t$$

If we assume an overall system efficiency (including reflectivity, quantum efficiency and other losses) of $NF\rho = 10^{-2}$ as before, then the effective energy per resolution element is

$$E_{eff} = 8 \times 10^{-16} E_t$$

The minimum detectable signal is of the order of 1 photon per resolution element or 1.9×10^{-19} joules per element. The signal to noise is then

$$S/N = 4.2 \times 10^{3} E_t$$

where E is the transmitted energy in joules. We have assumed that this energy is transmitted in the reciprocal of the doppler resolution time. For the 10 cm target, the doppler spread is $f = 10^{5} \Omega$ Hz, where Ω is the rotation rate. Assuming 10 doppler resolution elements, the resolution element $\Delta f = 10^{4} \Omega$ Hz, and the desired transmission time is $10^{-4}/\Omega$ seconds. For a 1-2 rps rotation rate, this time is of the order of ten microseconds. For a 1 rpm rate, it is approximately 1 millisecond. For a 1 watt average power YAG laser, the energy delivered in 1 millisecond is 10^{-3} joules which would put the reception of the image in the limit of detectability. For initial experiments, an artificial target with strongly retro-reflecting areas is being investigated.

At the present time, a mode-locked Nd:YAG laser is being fabricated for use in the imaging experiments. While this is being done, experiments have been conducted using doppler processing in conjunction with a scanning beam to obtain two dimensional images of laboratory targets.

The initial experimental configuration is shown in Fig. IV-1. The linearly polarized beam from a 1 milliwatt HeNe laser passes through a quarter wave plate which renders the beam circularly polarized. One polarization component is deflected by the calcete Glan-Thompson prism and serves as the local oscillator beam. The other component passes through the prism to the target. The lens couple and the rotating mirror provide a beam that translates in the horizontal plane. This beam is expanded in the vertical plane by means of a cylindrical telescope so that it provides a vertical strike beam that illuminates the entire vertical extent of the target. The reflected beam passes back through the transmitting optics and the polarizing prism. It then passes through the quarter wave plate, reflects off the laser output mirror, and after passing through the wave plate again, is restored to the same state of polarization as the local oscillator beam. It is then deflected by the prism and is focussed, together with the local oscillator beam on a PIN diode detector. This homodyne scheme has the advantage of being self-aligning.

The target itself consisted of a 5 cm diameter cylinder upon which was cemeted an array of pieces of reflecting tape. The cylinder axis was horizontal and the target was rotated about this axis at a rate of 0.5 rps. Due to the vertical expansion of the beam, the individual reflecting elements could not be resolved in the vertical direction by normal imaging. Since the doppler shift is proportional to the distance from the axis, however, resolution could be achieved by doppler processing. The horizontal resolution was provided by the horizontal scan of the beam.

The heterodyne signal, after passing through an appropriate preamplifier, was applied to a low frequency spectrum analyzer. The scan of the spectrum analyzer was synchronized with the rotation of the target. The output of the spectrum analyzer was used to modulate the intensity of a Tektronix 549 storage oscilloscope. The horizontal sweep of the oscilloscope was synchronized with the spectrum analyzer sweep. The vertical deflection of the oscilloscope was driven with the same sawtooth signal that was used to drive the scanning mirror. The amplitude of the signal was adjusted so that the beam traversed nearly the whole face of the oscilloscope during the scan of the laser beam across the target. Using this system, a well defined image of either the upper half or the lower half of the target could be obtained. (Only one half of the target could be observed at a time since the spectrum analyzer cannot distinguish positive and negative doppler shifts without a frequency offset of the local oscillator beam). In addition to the doppler ambiguity, this system suffers from a high noise level due to the low frequency fluctuations in the laser output and low frequency noise in the detection system.

The next system that was investigated is shown in Fig. IV-2. Here the LO signal is derived as previously. The second quarter wave plate causes the polarized component of the return signal to be deflected at the opposite side of the prism interface. In this configuration, the signal and LO beam are spatially separated so that they can be modified independently. The signal beam was passed through an acoustic modulator that was driven at a frequency of 40 MHz, and a power level of about 1 watt. This modulator shifted the frequency of the signal beam by 40 MHz with an efficiency of approximately 80%. The signal and LO beam were then recombined on a beamsplitter and detected by a PIN photodiode. The output of the PIN diode was fed to a low noise, high input impedance FET preamplifier, and then to a Tektronix 1L20 spectrum analyzer. The signal level and the impedance of the preamplifier were such that the dominant noise source was the shot noise of the LO beam, a condition necessary to achieve optimium signal to noise ratio. The output of the spectrum analyzer was used to intensity modulate the beam of the storage oscilloscope as has been described previously.

Using this system, well defined images of the reflector array on the target could be obtained. Typical images are shown in Fig. IV-3. In the upper image, the upper and lower edges of the target were not adequately illuminated by the vertical fan beam. The lower image shows essentially the entire front face of the target presented to the transmitter. The reflectivity pattern, as can be seen, consisted

of two rows of alternating square patches and one triangular patch. The horizontal and vertical axes of the image are reversed with respect to the physical axes of the target. The vertical axis of the image corresponds to the horizontal scan of the laser beam and resolution in this direction is provided by the scanning of the beam. The horizontal axis of the image corresponds to the vertical axis of the target and resolution in this direction is provided by the doppler processing done in the spectrum analyzer. The vertical line running through the image is a result of a small amount of feed through from the modulator driver and identifies the zero doppler shift point (the axis of the target). Each of the horizontal lines in the image correspond to a single sweep of the spectrum analyzer. The doppler spread in these images was approximately ± 200 KHz.

These images clearly demonstrate the very good spatial resolution that can be obtained by doppler processing (the width of the reflective patches in the vertical or doppler direction was about 0.5 cm). This resolution could, of course, have been obtained by normal imaging in the laboratory situation, but the resolution obtained by doppler processing in independent of range.

The next step in the investigation will be to use range-doppler processing to obtain two dimensional images rather than the scan-doppler processing used above. This investigation will use the short pulses obtainable from a mode-locked Nd:YAG laser to provide the down-range resolution. The simplest possible scheme, and the one that will be used for the initial experiments is shown in Fig. IV-4. Here the scanning mirror is replaced by the scanning optical delay line. In this configuration the transmitting optics will be arranged to illuminate the entire target with the stationary output beam. The remainder of the system will be similar to that shown in Fig. IV-1. Using this system one will obtain a range-doppler image on the storage oscilloscope.

These initial systems are quite inefficient from the standpoint of the use of the received optical energy. The spectrum analyzer processes the various frequency components of the return signal sequentially with consequent loss of signal to noise, i.e., while it is looking at one frequency resolution element, all the energy received in the others is ignored. The holographic type processing discussed in Section III does not suffer from this problem. A similar situation occurs with the scanning delay system shown in Fig. IV-4. It is expected that a considerable part of the effort in the next phase of the contract will be devoted to the investigation of more efficient signal processing techniques.

REFERENCE

IV-1. Massey, G. A.: Photomixing with Duffusely Reflected Light. Appl. Optics 4, pp. 781-784, July 1965.

FIG. IV-1

INITIAL DOPPLER RESOLUTION SYSTEM

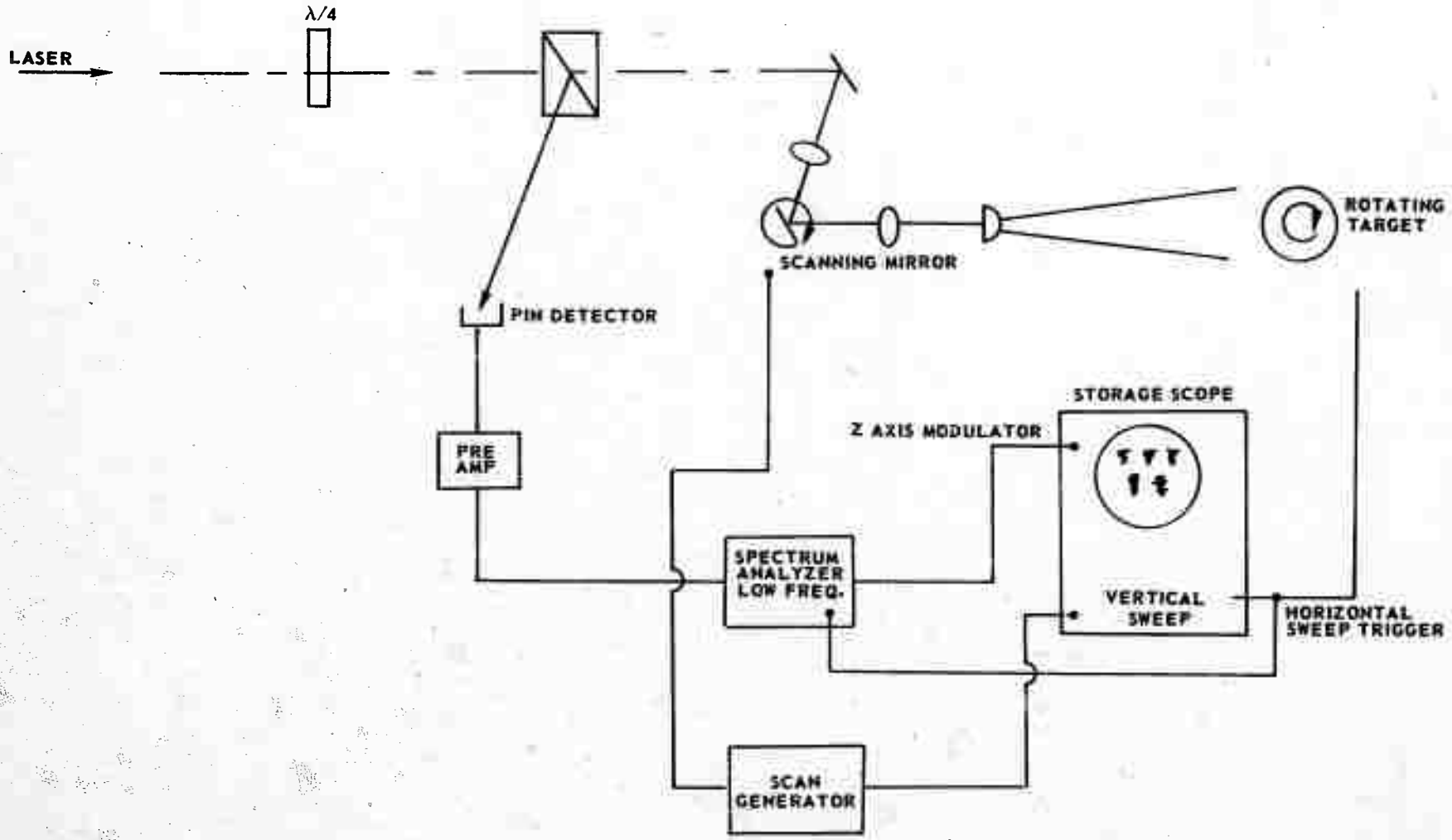

L920479-36

DOPPLER RESOLUTION SYSTEM

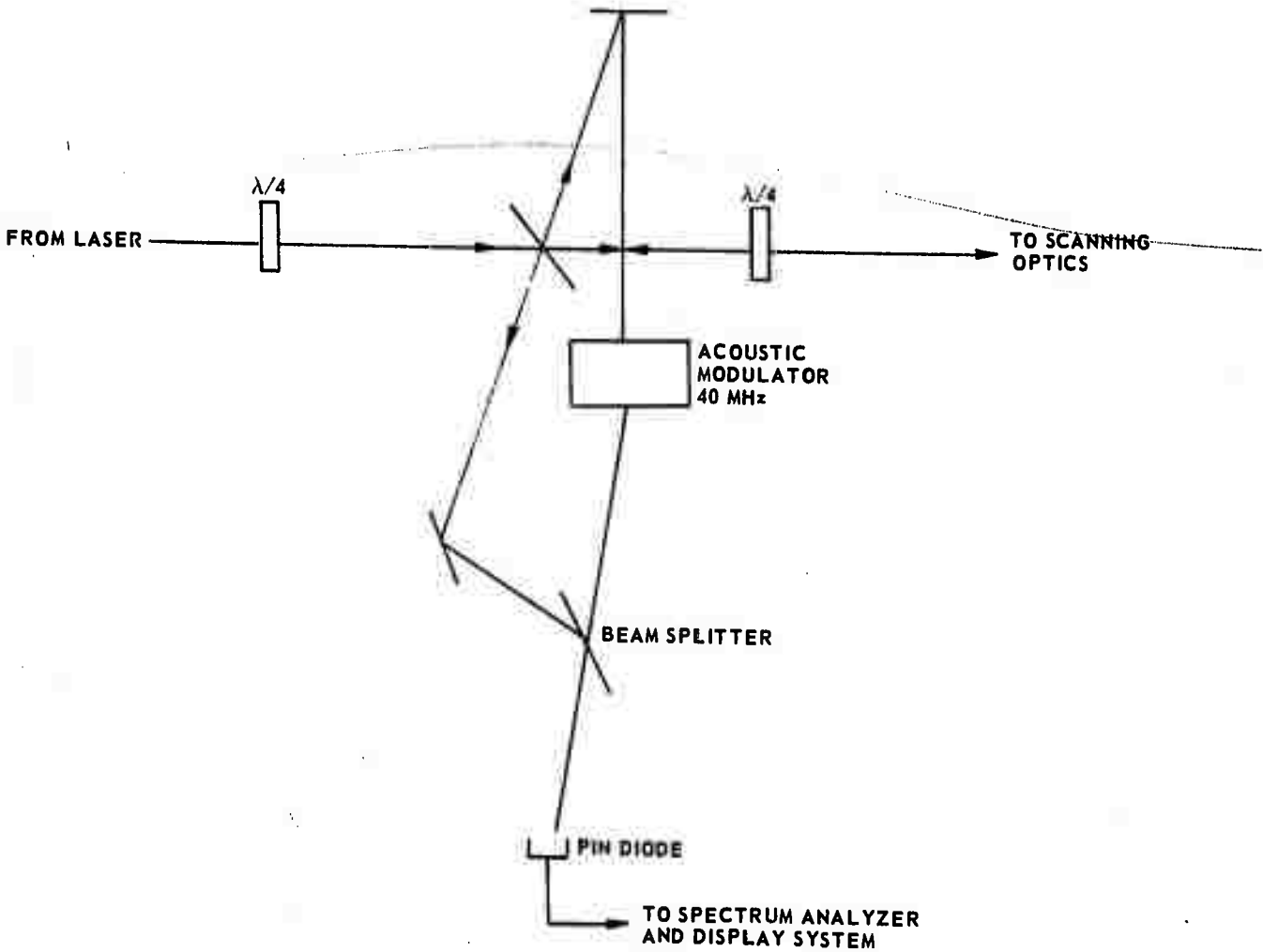

IMAGES OF LABORATORY TARGET

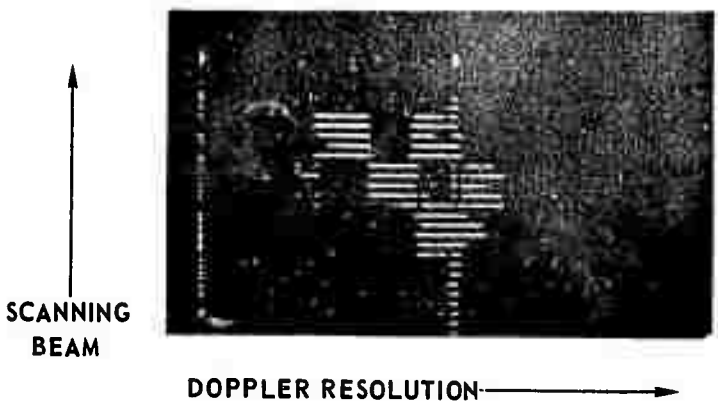

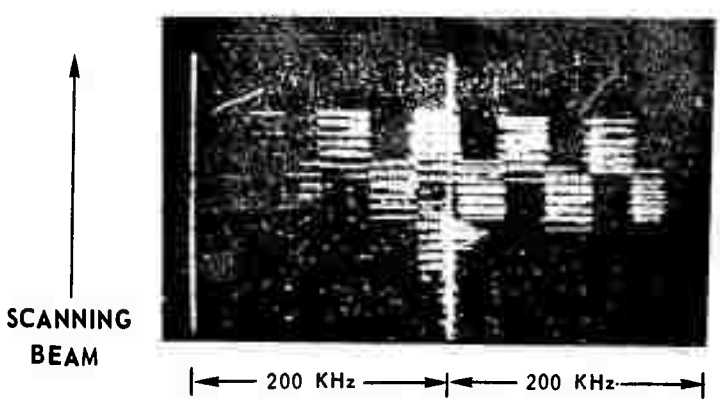

FIG. IV-4

SCHEMATIC RANGE-DOPPLER SYSTEM

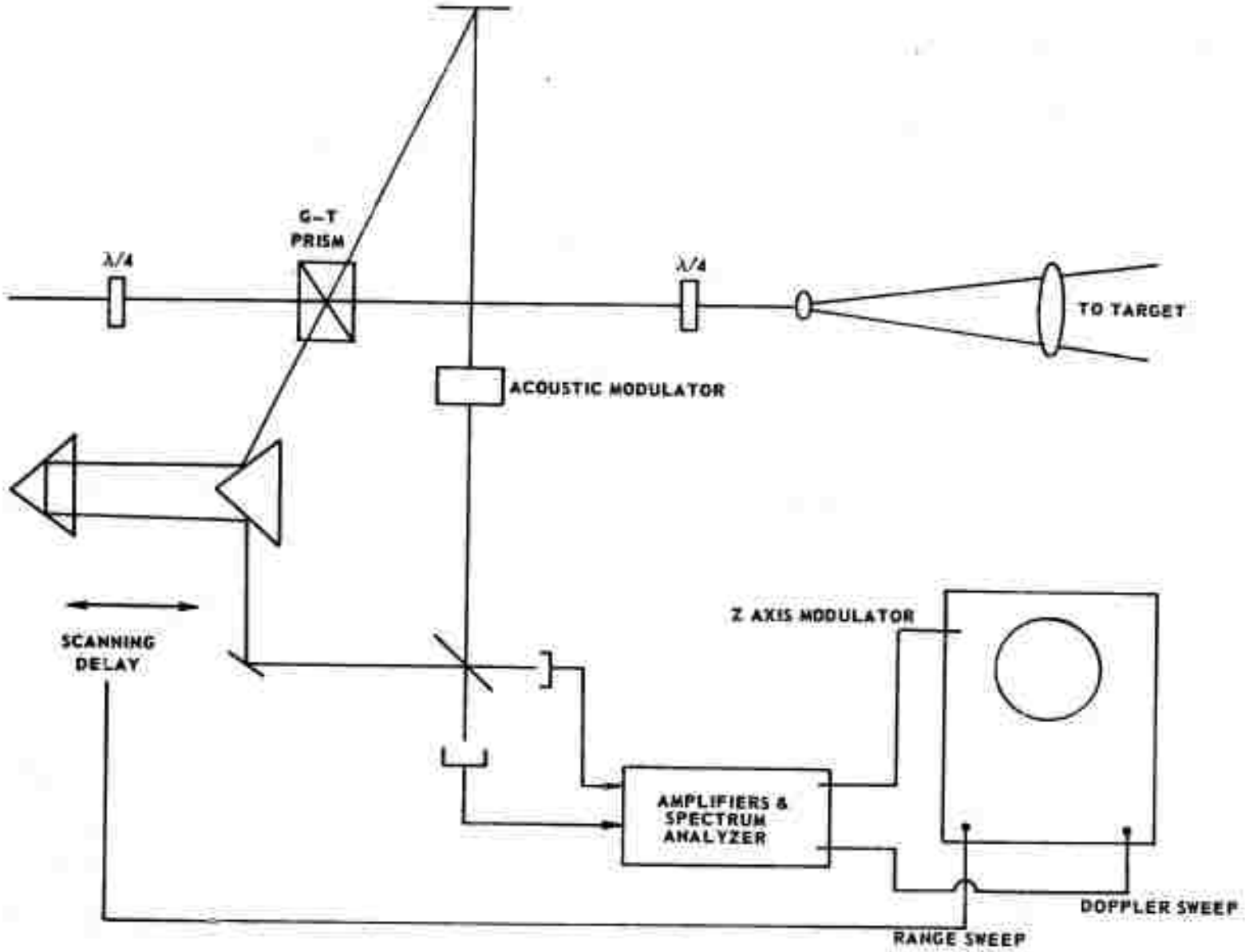

APPENDIX I

SINGLE-FREQUENCY TRAVELING-WAVE Nd:YAG LASER

by

A. R. Clobes

and

M. J. Brienza

Submitted for publication in Applied Physics Letters.

A Single-Frequency, Traveling Wave Nd:YAG Laser

by

A. R. Clobes and M. J. Brienza
United Aircraft Research Laboratories
East Hartford, Connecticut 06108

ABSTRACT

Single-frequency operation of a cw pumped Nd:YAG laser was achieved by using a ring cavity configuration containing a small differential loss. The resulting unidirectional traveling wave eliminated spatial hole burning, and the output of the laser was at a single-frequency.

A Single-Frequency, Traveling Wave Nd:YAG Laser

by

A. R. Clobes and M. J. Brienza
United Aircraft Research Laboratories
East Hartford, Connecticut 06108

Although the Nd:YAG laser transitions are homogeneously broadened, spatial hole burning[1] arising from standing waves in the laser cavity cause the output of the laser to be multifrequency. Previous methods of achieving single-frequency operation in the Nd:YAG laser involve the use of intracavity etalon mode selectors[2,3] movement of the laser rod relative to the standing wave pattern[4], or movement of the cavity standing wave pattern relative to the laser rod[5].

In the work to be described, single-frequency operation of a cw pumped Nd:YAG laser was achieved by using a ring cavity configuration containing a small differentia loss[6]. The resulting unidirectional traveling wave eliminated spatial hole burning, and the output of the laser was at a single-frequency.

The laser cavity configuration used in the experiments is shown in Fig. 1. A rectangular 4 mirror cavity was used for most of the experiments, although a 3 mirror triangular cavity worked equally well. With the rectangular cavity, three mirrors were coated for maximum reflectance, (one having a 10 m radius of curvature), and the fourth was either a 98 or 95 percent reflecting output mirror. The c/ℓ cavity frequency was 310 MHz. An iris was used to achieve single transverse mode operation. A 5 x 50-mm-Brewster-ended Nd:YAG rod was pumped with either a single Krypton arc or a tungsten filament lamp in an elliptical cavity.

The intracavity differential loss is based on the use of a Faraday rotator, consisting of a 5 cm length of fused quartz in a solenoid generated axial magnetic field, and a half-wave plate. The Faraday element rotated the cavity plane of polarization (defined by the Brewster-ended Nd:YAG rod), by a small angle $\pm\theta$; the sign being dependent on the propagation direction and polarity of the magnetic field. The half-wave plate was oriented with one of its axis at an angle $\beta/2$ with respect to the cavity plane of polarization. The magnetic field was such that for a wave traveling in the clockwise (cw) direction, the half-wave plate rotated the plane of polarization by an angle β and the Faraday cell by an angle $+\theta$, so that the total rotation was $(\beta + \theta)$, while the counterclockwise (ccw) wave experienced a rotation of $(\beta - \theta)$. Thus, the single pass intensity loss in the two waves, on passing through the Brewster face of the laser rod, was proportional to $\sin^2 (\beta + \theta)$ and to $\sin^2 (\beta - \theta)$ for the cw and ccw wave, respectively. The differential loss, Δloss, between the counter rotating waves was then:

$$\Delta\text{loss} \propto \sin^2 (\beta + \theta) - \sin^2 (\beta - \theta) \approx 4 \beta\theta$$

With the differential loss, the two counter circulating traveling waves were unstable; the wave with the lower loss increases in amplitude at the expense of the wave with the higher loss which therefore vanished[7] resulting in a unidirectional output from the laser, in this case, the ccw direction. For a maximum power output the half-wave plate and the intensity of the magnetic field on the Faraday rotator

are adjusted so that $\beta = \theta$. Then the entire loss, proportional to $4\theta^2$, is experienced only in the cw direction, leaving the ccw direction unattenuated. The resulting unidirectional traveling wave eliminated spatial hole burning and the homogeneously broadened line of the Nd:YAG laser oscillated in a single longitudinal mode.

The output of the laser was examined with an 8 GHz free spectral range scanning Fabry-Perot interferometer with a sweep rate of 2.0 GHz/msec. In addition, single-frequency operation of the laser was verified by detecting the laser output with a high-speed photodiode, the output of which as displayed on a wideband spectrum analyser (HP Model 8551B). Absence of all rf cavity beat frequencies confirmed single-frequency operation. The total output power was measured with a calibrated thermopile.

Shown in Fig. 2 is a Fabry-Perot display of the laser output. With no magnetic field on the Faraday rotator, the laser output was multifrequency covering a range of approximately 1 GHz. This relatively narrow oscillating line width is characteristic of the ring laser with a Brewster-ended Nd:YAG rod. The axis of the flat-ended Faraday cell and the half-wave plate were misaligned relative to the optical beam so that neither of these elements was a mode selecting etalon. With a magnetic field of 100 gauss, single-frequency output was obtained in one direction, with the residual power output in the reverse direction at least 30 db lower. Fabry-Perot inspection of the residual output confirmed that it also was at a single-frequency. The applied magnetic field on the Faraday element rotated the plane of polarization of one traveling wave by approximately 20 minutes, and the

resulting single-pass differential loss was less than .01 percent. The modest magnetic field required for single-frequency operation are well within the capabilities of small permanent magnets. Reversal of the polarity of the magnetic field reversed the direction of oscillation of the laser.

Increased amplitude and frequency stability of the single-frequency, traveling-wave laser relative to a multifrequency laser was also observed. A typical frequency stability over a 10-second time period was better than 80 MHz, and the amplitude stability over the same time period was better than 2 percent.

The single-frequency power output of the laser was greater than the total multifrequency power output previously obtained in both directions; the only experimental difference being the presence or absence of the magnetic field on the Faraday cell. The amount of increase depended on the pumping level. For the pump level near threshold, the single-frequency power was approximately $1\frac{1}{2}$ times the total multifrequency output while for high pump levels the increase was approximately 10 percent. This increase of output power in going from a standing to a traveling wave condition at the low pump levels had been predicted by J. A. White[7,8]. The fact that the power output of the laser increases from the multifrequency to the single-frequency operation verifies that it was possible to attenuate one of the traveling waves without attenuating the counter rotating component. Single-frequency, cw, fundamental transverse mode power output of 3/4 watt was readily achieved from this laser with an input power of 2,100 watts into the Krypton arc lamp.

A Brewster-ended laser rod was necessary for the operation of the single-frequency, traveling wave ring laser in order to eliminate etalon effects of a flat-ended laser rod which occur even though the ends of such a rod are anti-reflection (< .2 percent reflectance) coated. The etalon properties of a flat-ended laser rod were apparent in a Fabry-Perot display of the laser output where it was observed that the optical modes of such a laser were spaced by multiples of the $c/2n\ell$ frequency of the rod. The existence of the etalon effect implies a standing wave in the laser rod which we found could not be completely eliminated even by placing a differential loss element in a ring cavity. At best, two mode unidirectional operation of the laser resulted in which the modes were separated by the $c/2n\ell$ frequency of the laser rod. The power output of one mode was typically 3 to 5 times the power output of the second mode.

Since Nd:YAG is an effective Faraday rotator in an axial magnetic field, the laser rod itself was used as the differential loss element with the reciprocal rotation which previously was provided for by the half-wave plate, now provided by the induced birefringence[9] in the laser rod. A 1,500 watt tungsten filament lamp was used as the optical pump while the magnetic field was generated by a solenoid wrapped around the pump cavity. A magnetic field of 200 gauss was adequate to achieve single-frequency operation. The use of the laser rod as the differential loss element resulted in a very simple cavity configuration, since no additional intracavity optical elements were required.

Q-switched operation of the single-frequency Nd:YAG laser by means of an acousto-optic Bragg cell has also been achieved. The acoustic cell was fabricated of flint glass with a bonded transducer, operating at 40 MHz. The acoustic cell when placed in an axial magnetic field served as both a Q-switching element and a Faraday rotator. In the initial experiments, single-frequency Q-switching pulses having a peak power of 300 watts and 0.5 μ sec duration were obtained.

The authors would like to thank A. J. DeMaria for his encouragement and to C. Bardons for his technical assistance.

REFERENCES

(1) C. L. Tang, H. Statz, and G. DeMars, J. Appl. Phys., 34, 2289 (1963).

(2) M. Hercher, Appl. Opt., 8, 1103 (1969).

(3) H. G. Danielmeyer, IEEE Jour. of Quantum Electronics, QE-6, 101 (1970).

(4) H. G. Danielmeyer and W. G. Nilsen, Appl. Phys. Letters, 16, 124 (1970).

(5) H. G. Danielmeyer and E. H. Turner, Appl. Phys. Letters, 17, 519 (1970).

(6) A. L. Mikaeliane, J. G. Turkov, V. F. Kuprishov, V. J. Antonyanz and V. I. Kruglov, IEEE Conference on Laser Engineering and Applications. Digest of Technical Papers, Paper 10.8 (1969). IEEE Jour. of Quantum Electronics, QE-5, 617 (1969).

(7) J. A. White, Jour. Appl. Phys., 137, A1651 (1965).

(8) J. A. White, Nature, 201, 911 (1964).

(9) W. Koecher and D. K. Rice, IEEE Jour. of Quantum Electronics, QE-6, 557 (1970).

FIGURE CAPTIONS

Figure 1: Single-frequency, traveling-wave Nd:YAG laser cavity configuration.

Figure 2: Fabry-Perot display of laser output. 8 GHz free spectral range.

(a) Unidirectional operation, B = 100 gauss 20 mv/div vertical scale.

(b) Bidirectional operation, B = 0 20 mv/div vertical scale.

20 mV/div

a) UNIDIRECTIONAL LASER B=100 gauss

20 mV/div

b) BIDIRECTIONAL LASER B=0

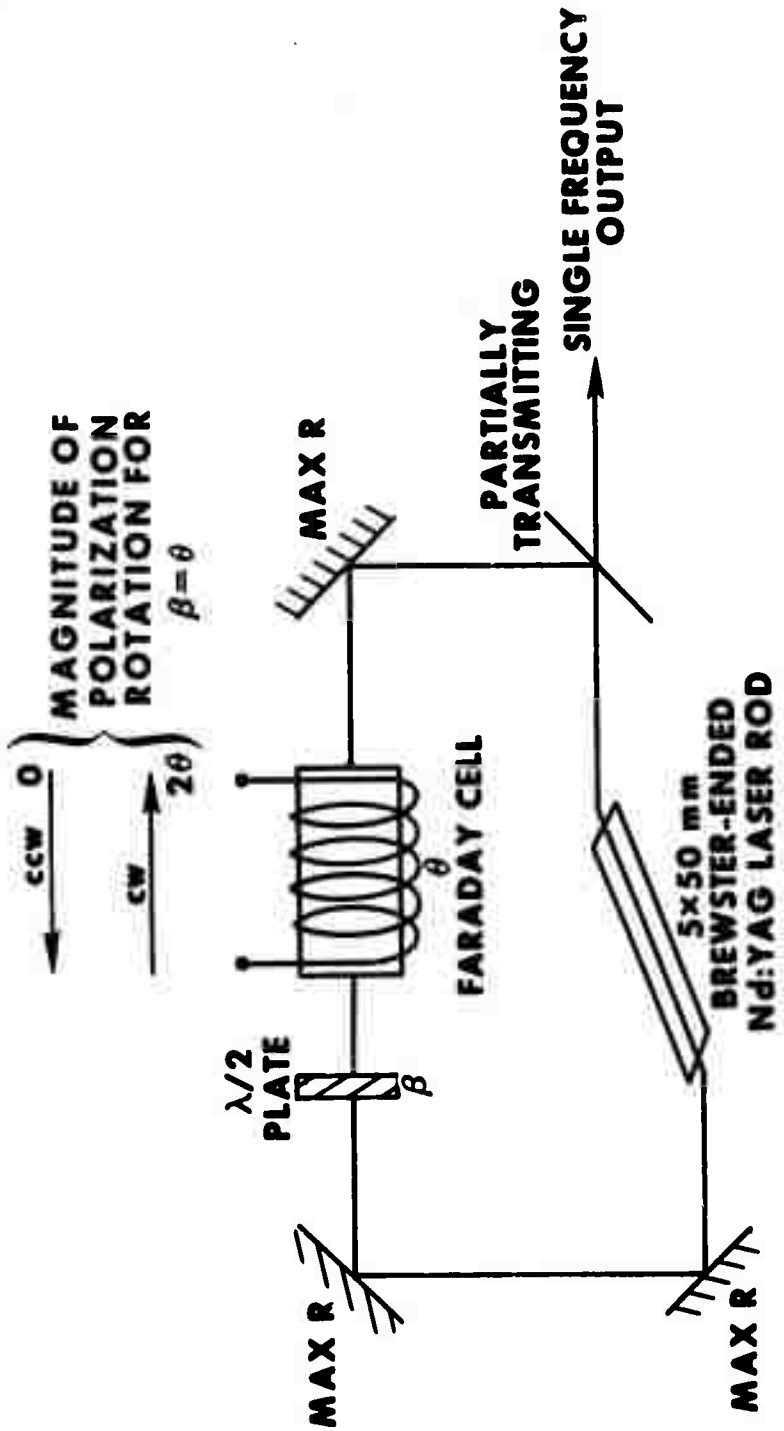
MAGNITUDE OF POLARIZATION ROTATION FOR $\beta=\theta$
ccw 0
cw 2θ
MAX R
PARTIALLY TRANSMITTING
SINGLE FREQUENCY OUTPUT
θ
FARADAY CELL
5×50 mm BREWSTER-ENDED Nd:YAG LASER ROD
$\lambda/2$ PLATE
β
MAX R
MAX R